A Case Study of Explosive Subsynoptic-Scale Cyclogenesis

JOHN R. GYAKUM AND EARL S. BARKER*

Department of Atmospheric Sciences, University of Illinois, Urbana, Illinois

(Manuscript received 24 August 1987, in final form 26 April 1988)

ABSTRACT

The continental cyclone of 28–29 March 1984 was noteworthy for its explosive intensification within six hours. Surface and upper-air data are analyzed for this storm throughout its 18-h life cycle of growth and decay over the eastern United States. The short time scale of this low's explosive development motivates us to place particular emphasis upon the hourly surface observations and their relationship to the rapid cyclogenesis.

While the synoptic-scale environment of the cyclogenesis consisted of quasi-geostrophic ascent, surface data reveal that the intersection of a heated moist tongue of air and an intensifying cold front was the approximate location of the initial vortex. The surface-based lifted index over the incipient cyclone was about −8°C. Static stability had decreased steadily prior to the cyclogenesis. Frontogenetic forcing and deep convection followed the surface cyclone for the next four hours of explosive deepening.

Filling of the cyclone occurred as the surface frontogenetic forcing eased, and the convection was displaced from the cyclone's center. The second pulse of explosive deepening ensued as an axis of maximum 500-mb cyclonic vorticity advection passed over the surface low.

This study shows that several physical processes, of differing scales, combine synergistically to effect this rare case of explosive land cyclogenesis.

1. Introduction

The continental United States cyclone of 28–29 March 1984 has left a rich meteorological legacy for us to study. This system, as it moved northeastward from its origin in eastern Alabama, spawned 22 tornadoes, produced rainfall in excess of 60 mm, contained sustained winds of 20 m s^{-1}, deepened 12 mb during one 4-h period, and was responsible for record low pressures throughout the Middle Atlantic states. The cyclone passed directly over Athens, Georgia and a remarkable horizontal pressure gradient is illustrated by the location's barogram (Fig. 1). Some of the extreme pressure changes observed in this barogram are associated with a strong thunderstorm collocated with this incipient cyclone. Indeed, we will see a strong association of the cyclone and convection throughout much of its early development. The pressure fall exceeding 16 mb in the 5 h preceding 2000 UTC 28 March 1984 is reminiscent of the extreme barogram-documented pressure falls shown by Gyakum (1983a) and Reed and Albright (1986) to exist in the more common maritime "bombs" (Sanders and Gyakum 1980). These studies have also suggested an association of cumulus convection and explosive cyclogenesis.

Our objective is to study the evolution of this rare case of explosive continental cyclogenesis during its 18-h history, before it moved offshore. The central pressure time trace (Fig. 2) for this 18-h period shows two periods of rapid deepening separated by a 6-h hiatus. Although the net 12-mb pressure fall during the 12-h period beginning at 1800 UTC 28 March shows this case to be a marginal "bomb" according to Sanders and Gyakum (1980), the central pressure fall rates over shorter time intervals are substantially greater than that found over 12 h. The relative wealth of hourly surface and 12-hourly upper-air data, as opposed to the paucity of meteorological reports typically surrounding an explosively-developing oceanic cyclone, affords us a unique opportunity to examine a bomb. We hypothesize that many of the same physical processes, so crucial to explosive oceanic cyclogenesis, are operating in this explosive land case.

The explosive cyclogenesis problem has received significant attention since 1980. Bosart (1981), Bosart and Lin (1984), and Uccellini et al. (1984, 1985) have presented observational and diagnostic studies of the Presidents' Day cyclone of 1979. The *QEII* cyclone of 1978 has been examined both observationally (Gyakum 1983a,b; Uccellini 1986) and numerically (Anthes et al. 1983). Reed and Albright (1986) have examined a case of extreme maritime cyclogenesis in the eastern Pacific. These studies have focused upon a variety of physical processes as possible culprits in the

* Current affiliation: Harris Corporation, Bellevue, NE 68005.

Corresponding author address: Professor John R. Gyakum, Dept. of Meteorology, McGill University, 805 Sherbrooke Street West, Montreal, Quebec H3A 2K6, Canada.

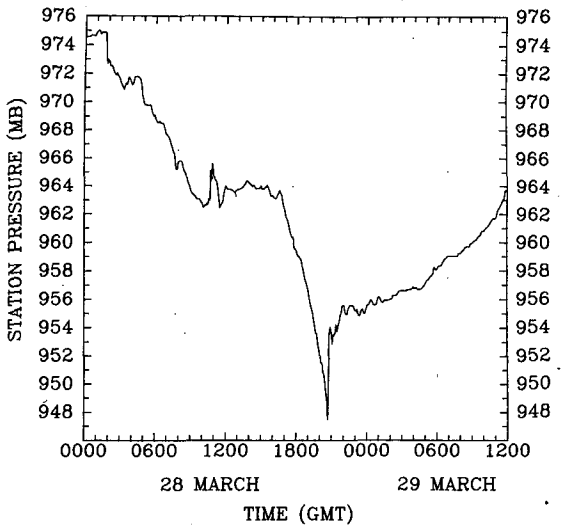

FIG. 1. Barogram for Athens, Georgia, for the period 0000 UTC 28 March through 1200 UTC 29 March 1984. The station pressure is recorded each 5 min.

explosive cyclogenesis. These have included baroclinic instability in the presence of weak static stability (Reed and Albright 1986), upper tropospheric jet streaks (Uccellini et al. 1984; Uccellini 1986), and the emphasis upon boundary-layer induced diabatic processes (Bosart 1981; Gyakum 1983b). Roebber's (1984) recent statistical study of cyclogenesis has suggested that a physical mechanism, or mechanisms, distinct from the usual baroclinic instability, may be responsible for the development of "bombs".

An inhibiting factor in previous observational studies of explosive cyclogenesis is that good data coverage is rarely sufficiently frequent to diagnose these extremely rapid developments. The extensive hourly surface and 12-hourly radiosonde data coverage in this case allows us to examine plausible physical mechanisms potentially responsible for this rare land cyclogenesis case. Section 2 examines the synoptic environment surrounding the cyclogenesis. Section 3 describes the surface mesoscale cyclone and its relationship to convection. The role of fronts is explored in section 4, while a thermodynamic and potential vorticity analysis is performed in section 5. Forecast implications are discussed in section 6, followed by a concluding discussion in section 7. All locations and three-letter identifiers discussed in this paper are shown in Fig. 3.

2. Synoptic environment

Manually analyzed sea-level pressure, 1000–500 mb thickness, and 300-mb charts are shown in Figs. 4 through 6 for the 24-h period beginning at 1200 UTC 28 March 1984. At this time, several surface low pressure centers exist in the southeastern United States. These lows form the center of a cyclonic circulation covering the entire eastern United States, except for a cool surface ridge extending from Maine southwestward to eastern North Carolina. Extremely warm temperatures were observed in south Texas the previous day with Brownsville reporting a record high of 41°C, while areas in the Texas panhandle had surface temperatures of only 4°C. The surface front, along which the explosive mesocyclone develops at 1800 UTC, extends south-southwestward from a low centered in western Tennessee. A 300-mb jet exceeding 65 m s^{-1} extends through the strong baroclinic zone and thickness trough region from Texas into western Mississippi. There is strong upper-level support for much of the surface cyclonic system, as it is located downstream, and on the cyclonic side of the powerful 300-mb jet.

The numerous missing wind reports at 300 mb, throughout the cyclone's existence, attest to the difficulty of accurately documenting the upper tropospheric wind field. To alleviate this problem, we computed gradient winds for each missing mandatory-level rawinsonde observation. These gradient winds, while not displayed in Figs. 4 through 6, are used in the isotach analyses and in all objective analyses involving winds.

By 0000 UTC 29 March (Fig. 5), the intense 975 mb mesocyclone that had formed at 1800 UTC in eastern Alabama, is seen at the North Carolina–South Carolina border. The weaker lows found in West Virginia and extreme western Virginia are the remnants of those systems previously found in the respective states of Kentucky and Tennessee. The surface low is located along a strong frontal system with the cool surface ridge to its northwest and record warmth to its southeast. The surface low also is in a good location for continued development as it is on the downstream cyclonic side of the 300 mb jet. The pressures have

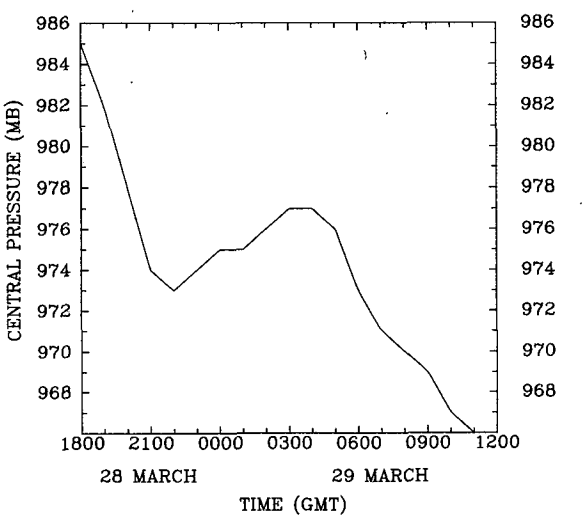

FIG. 2. Central pressure (mb) of the surface cyclone, as a function of time through 1200 UTC 29 March. This plot is derived from hourly altimeter setting analyses.

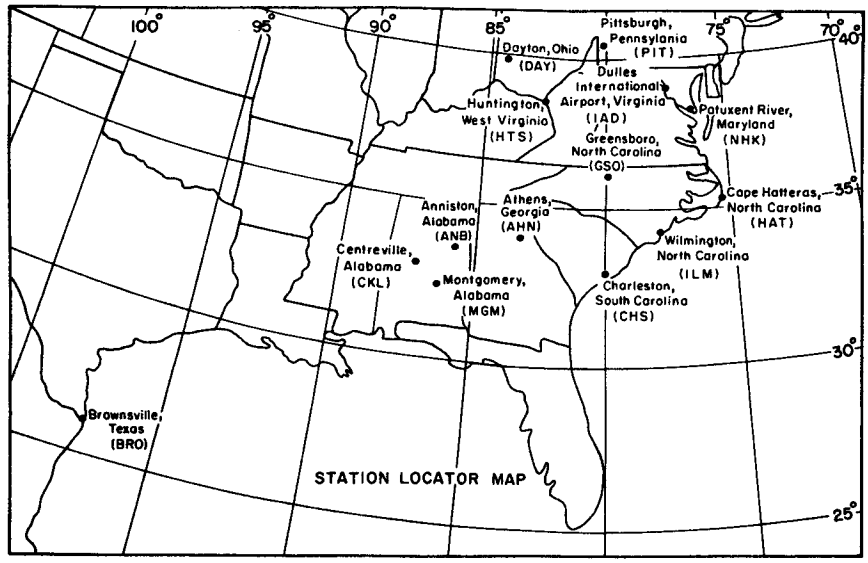

FIG. 3. Station locator map for all locations discussed in text.

fallen substantially throughout the environment surrounding this cyclone. This condition was clearly observed by Uccellini et al. (1984) and by Reed and Albright (1986) in other cases of explosive cyclogenesis.

By 1200 UTC 29 March, the surface mesocyclone (Fig. 6) had intensified to 966 mb. Remnants of the cool surface ridge are still seen from north of the cyclone center to Maine. At this mature stage of the cyclone, the surface low is nearly collocated with the 300 mb closed low. A mesoscale 1000–500 mb thickness ridge, seen at 0000 UTC, still exists over the surface low.

To better understand the synoptic patterns just seen, we present a quasi-geostrophic vertical velocity diagnosis for the case. This quasi-geostrophic ω-equation may be written as

$$\sigma\nabla^2\omega + f^2\frac{\partial^2\omega}{\partial p^2} = -2\nabla\cdot\mathbf{Q} \qquad (1)$$

where the static stability,

$$\sigma = \frac{-R}{P}\left(\frac{P}{P_0}\right)^{\kappa}\left[\frac{\partial\theta}{\partial P} - \left(\frac{\partial\theta}{\partial P}\right)_{\mathrm{ma}}\right],$$

is a function of pressure only, and

$$\mathbf{Q} = \left\{-\frac{R}{P}\frac{\partial \mathbf{v}_g}{\partial x}\cdot\nabla T_v, -\frac{R}{P}\frac{\partial \mathbf{v}_g}{\partial y}\cdot\nabla T_v\right\}.$$

Additionally, the static stability is computed assuming a completely saturated atmosphere with moist adiabatic (ma) vertical displacements. All symbols are defined in the Appendix.

Hoskins et al. (1978) and Hoskins and Pedder (1980) have shown that quasi-geostrophic ascent and descent are forced by, respectively, convergence and divergence of **Q**. These **Q**-vectors may be easily calculated on constant pressure surfaces, because their computation requires only a knowledge of virtual temperature and geopotential height. Our analysis is based upon **Q**-vector computations at 850, 700, 500 and 300 mb.

Fields of temperature, dewpoint, and geopotential height are objectively analyzed to a one degree latitude–longitude grid. The objective analysis is based upon the method of Barnes (1973) so that weighting functions are computed for each of ten observations closest to a given gridpoint. The weighting function exponentially decreases from one at zero distance to 0.1 at the average distance of these ten stations from the gridpoint. Centered finite differencing is used to compute derivations at each grid point.

Figure 7 shows **Q**-vectors and quasi-geostrophic ω from Eq. (1) at 850 and 500 mb for the 24-h period beginning at 1200 UTC 28 March 1984. The vertical velocities are assumed to vanish at 1000 and 100 mb. Thus, pressure-weighted corrections to the vertical velocities are applied at each level.

As 1200 UTC 28 March, an extensive area of ascent (Fig. 7.) covers the eastern United States at both 850 and 500 mb, in association with the large surface cyclonic system discussed earlier (Fig. 4a). The most notable difference between the two levels is that an axis of strong 500 mb ascent extends from southern Missouri to the southern Louisiana coast, just to the west of the developing surface trough (Fig. 4a). Strong ascent in this region is absent at 850 mb. The 500 mb ascent is in response to a vigorous upper tropospheric trough seen in eastern Texas (Fig. 4b).

By 0000 UTC 29 March 1984, substantial 850 mb ascent (Fig. 7) is seen over and to the northeast (in a

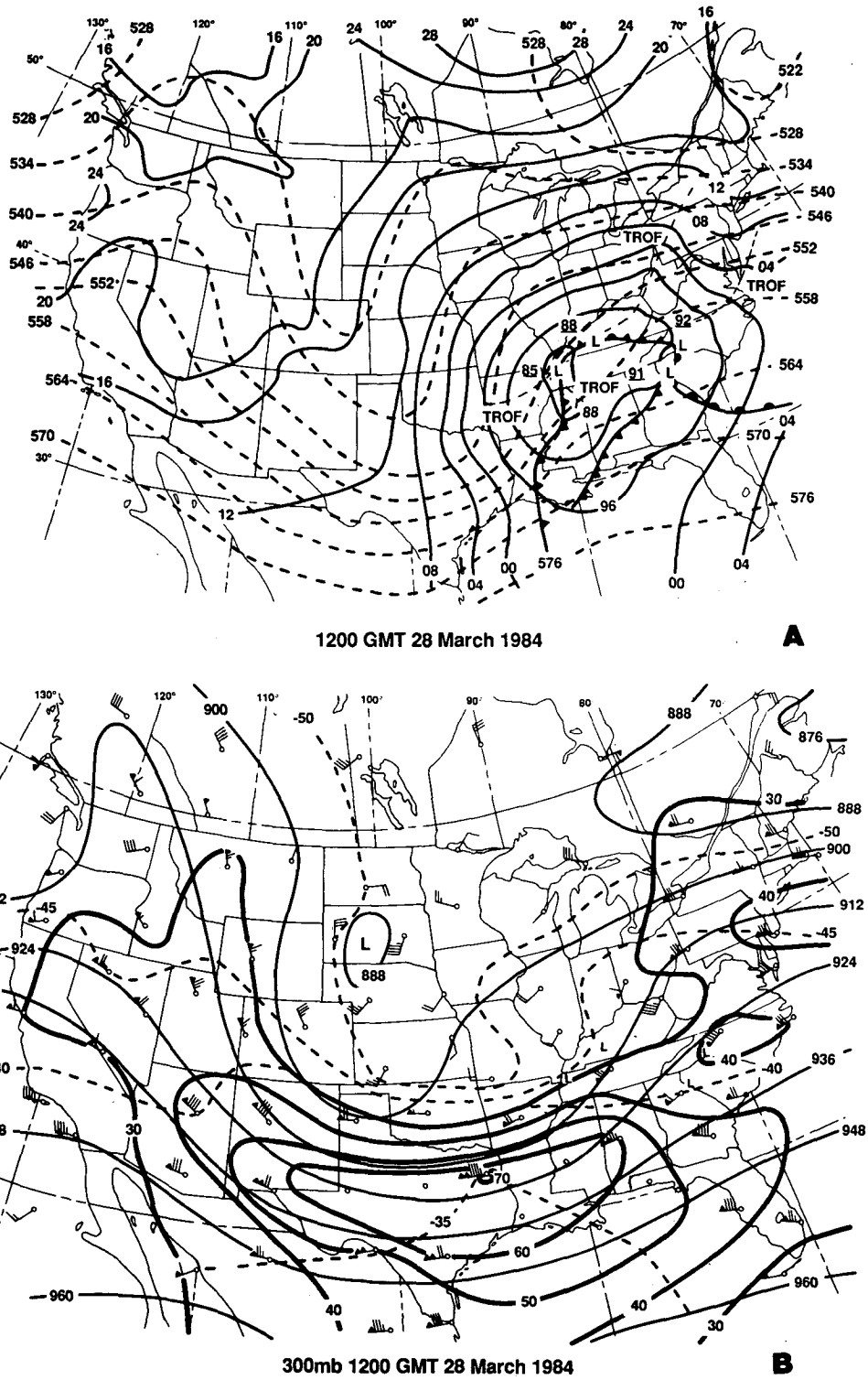

FIG. 4. (a) Sea-level pressure (solid, mb with hundreds and thousands digits omitted), and 1000–500 mb thickness (dashed, dam) chart for 1200 UTC 28 March 1984. Contour intervals for pressure and thickness are, respectively, 4 mb and 6 dam. (b) 300-mb height (dam), temperature (°C), and isotach (m s^{-1}) analyses for wind speeds in excess of 30 m s^{-1}. Conventionally plotted data are also shown with winds (m s^{-1}) [full (half) barb = 5 (2.5) m s^{-1} and pennant = 25 m s^{-1}]. Station circle is darkened when the dewpoint depression ≤5°C. Surface lows are also indicated as small L's on charts.

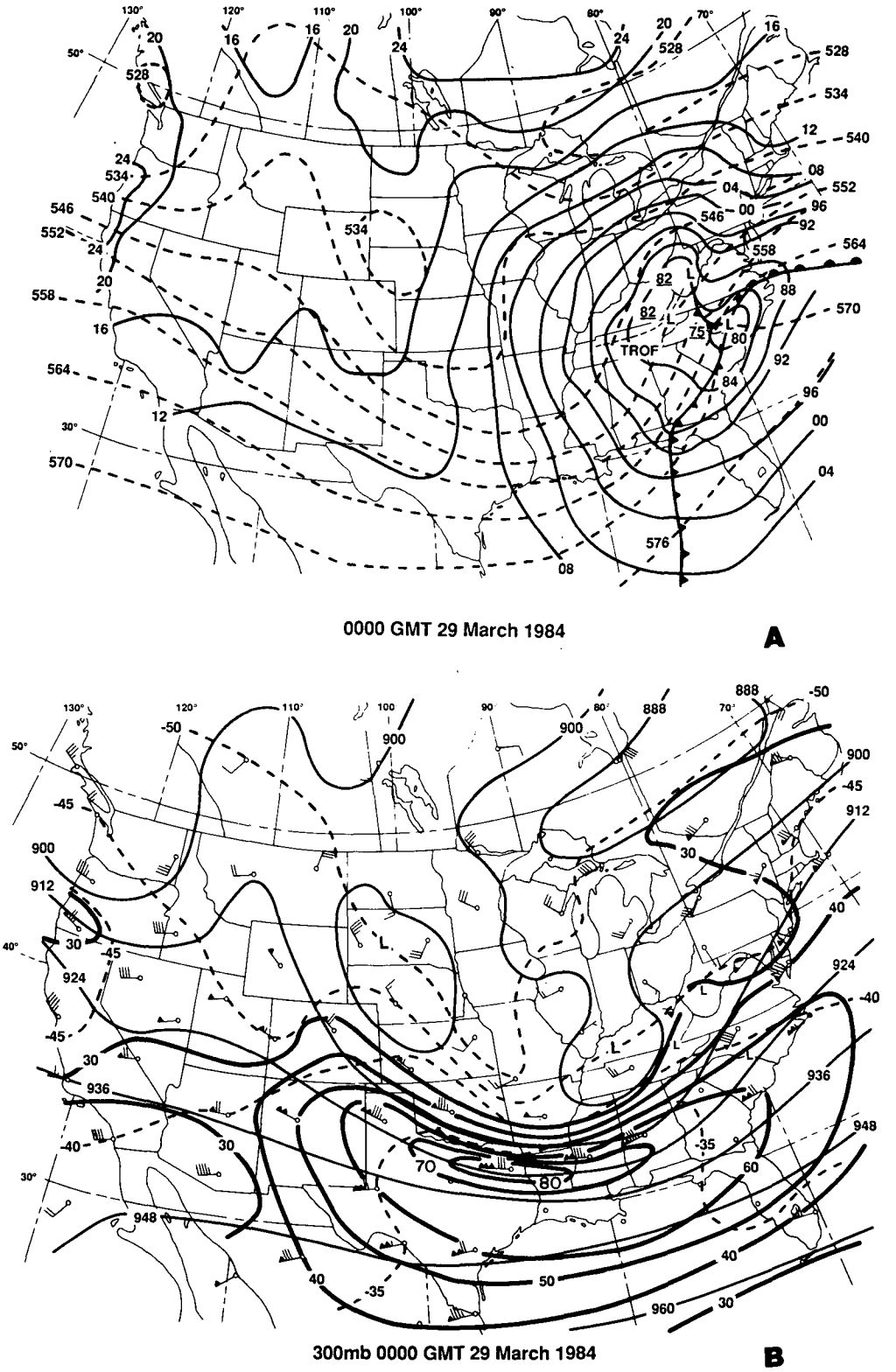

FIG. 5. As in Fig. 4, except for 0000 UTC 29 March 1982.

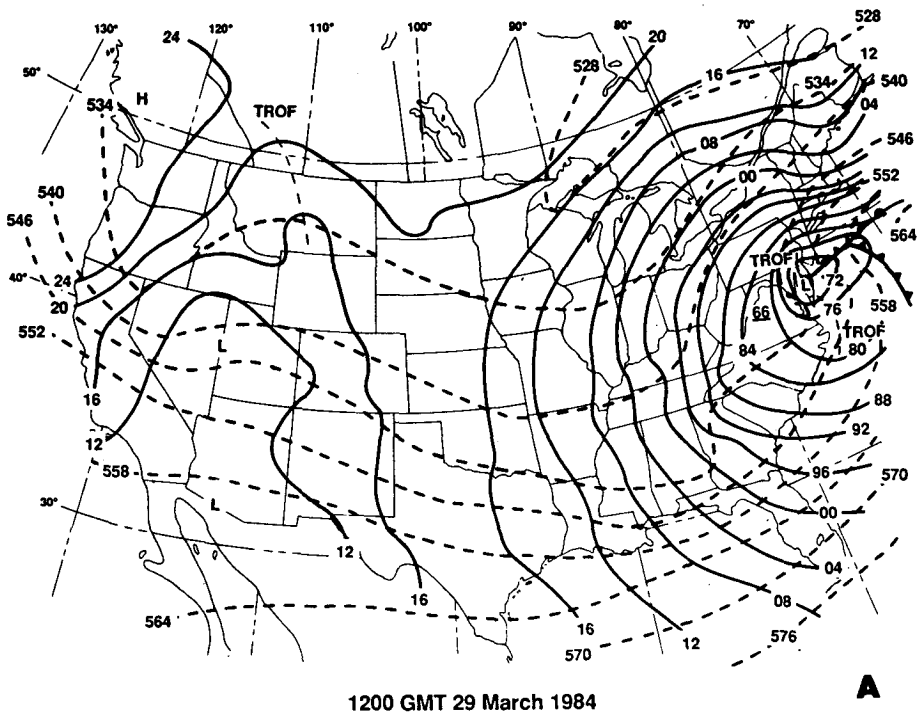

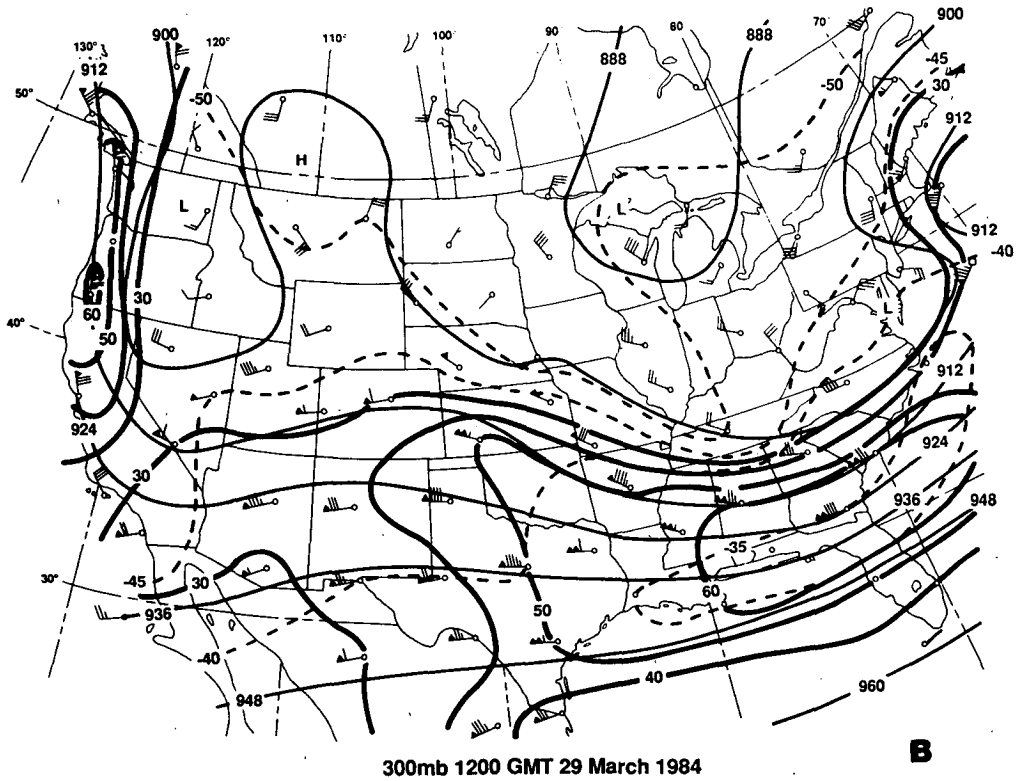

FIG. 6. As in Fig. 4, except for 1200 UTC 29 March 1982.

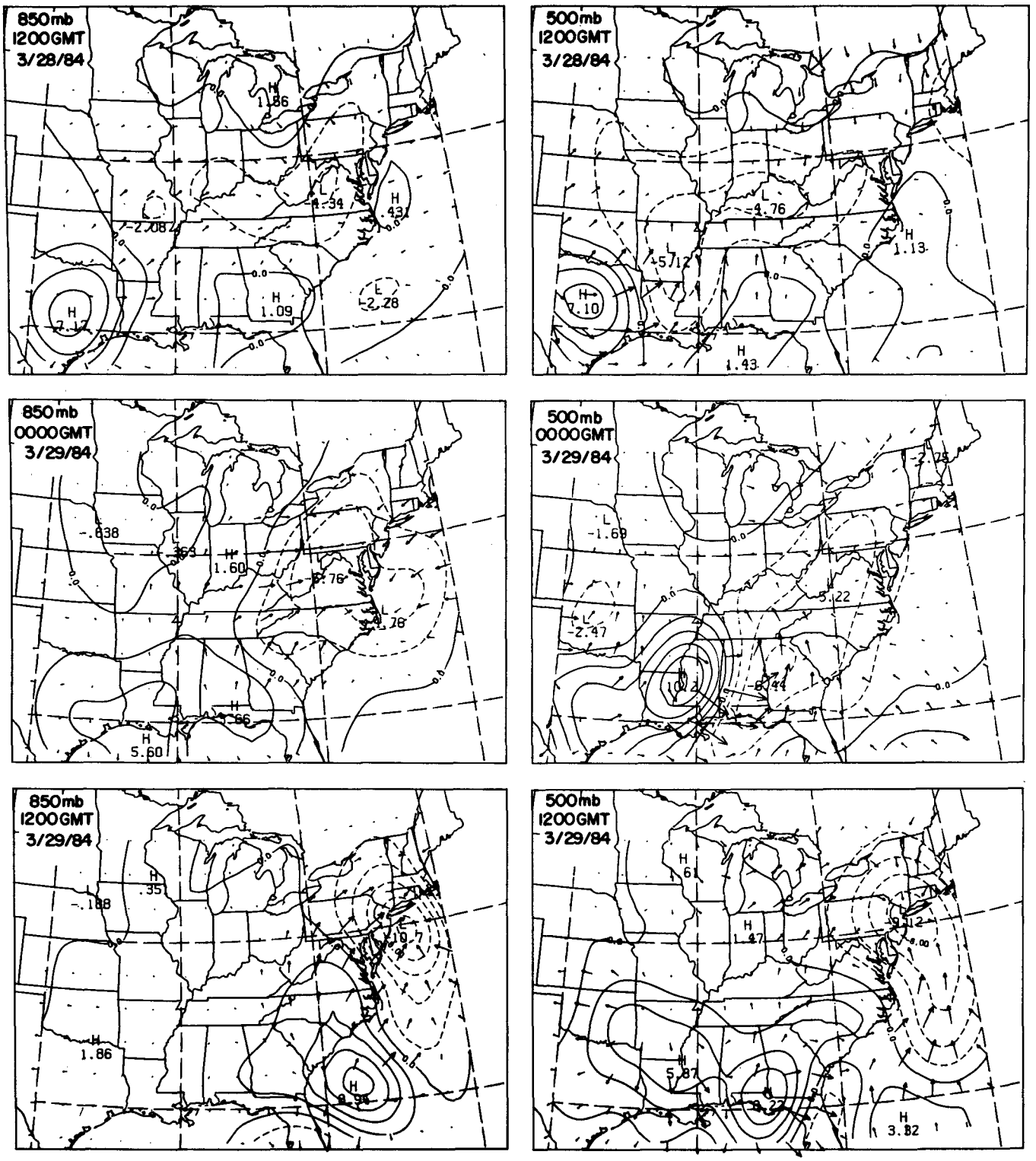

FIG. 7. Quasi-geostrophic vertical velocity and Q-vector analysis for 850 and 500 mb at 1200 UTC 28 March 1984 and 0000 and 1200 UTC 29 March 1984. Vertical motion contours are shown every 1 $\mu b\ s^{-1}$ with negative (ascent) contours dashed. Q-vectors, as defined in (1), are plotted each 2° of latitude and longitude. An arrow length of 2° latitude corresponds to 5.0×10^{-10} m s^{-3} mb^{-1}.

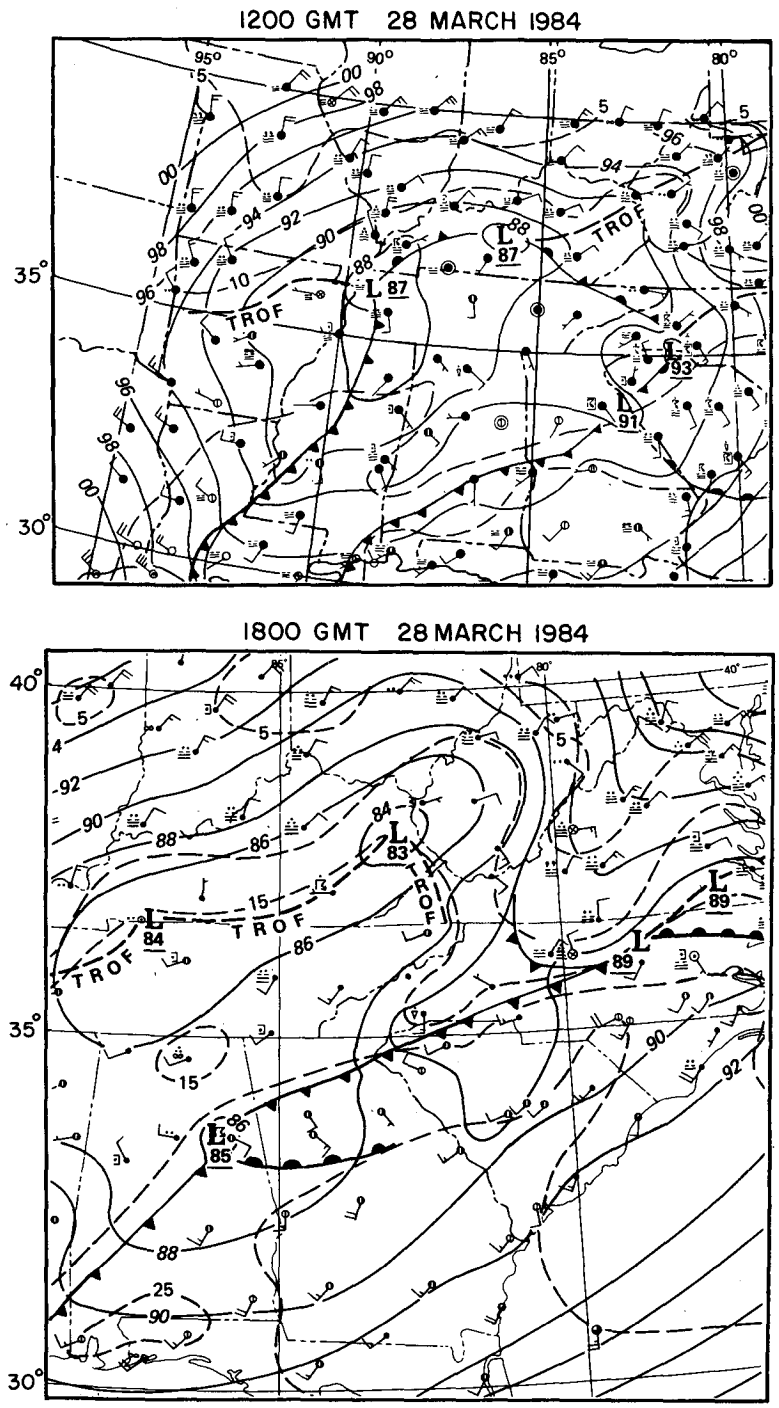

FIG. 8. Surface sectional analyses for 1200, 1800 and 2100 UTC 28 March and 0000, 0600 and 1200 UTC 29 March 1984. Analyzed pressures (solid) are altimeter settings converted to mb, and temperatures (dashed) are in °C. Weather observations are plotted conventionally. Heavy dashed lines indicate troughs. Wind plotting convention follows that of Fig. 4.

region of geostrophic warm advection) of the intense 975 mb surface cyclone (Fig. 5). In contrast, the strongest 500 mb ascent lies to the southwest of the surface cyclone, just to the east of the vigorous 300-mb trough and strong jet in southern Mississippi.

At 1200 UTC 29 March, the ascent patterns at both 500 and 850 mb (Fig. 7) are similar with substantial quasi-geostrophic ascent now extending throughout the troposphere over and slightly to the east of the 966 mb cyclone (Fig. 6).

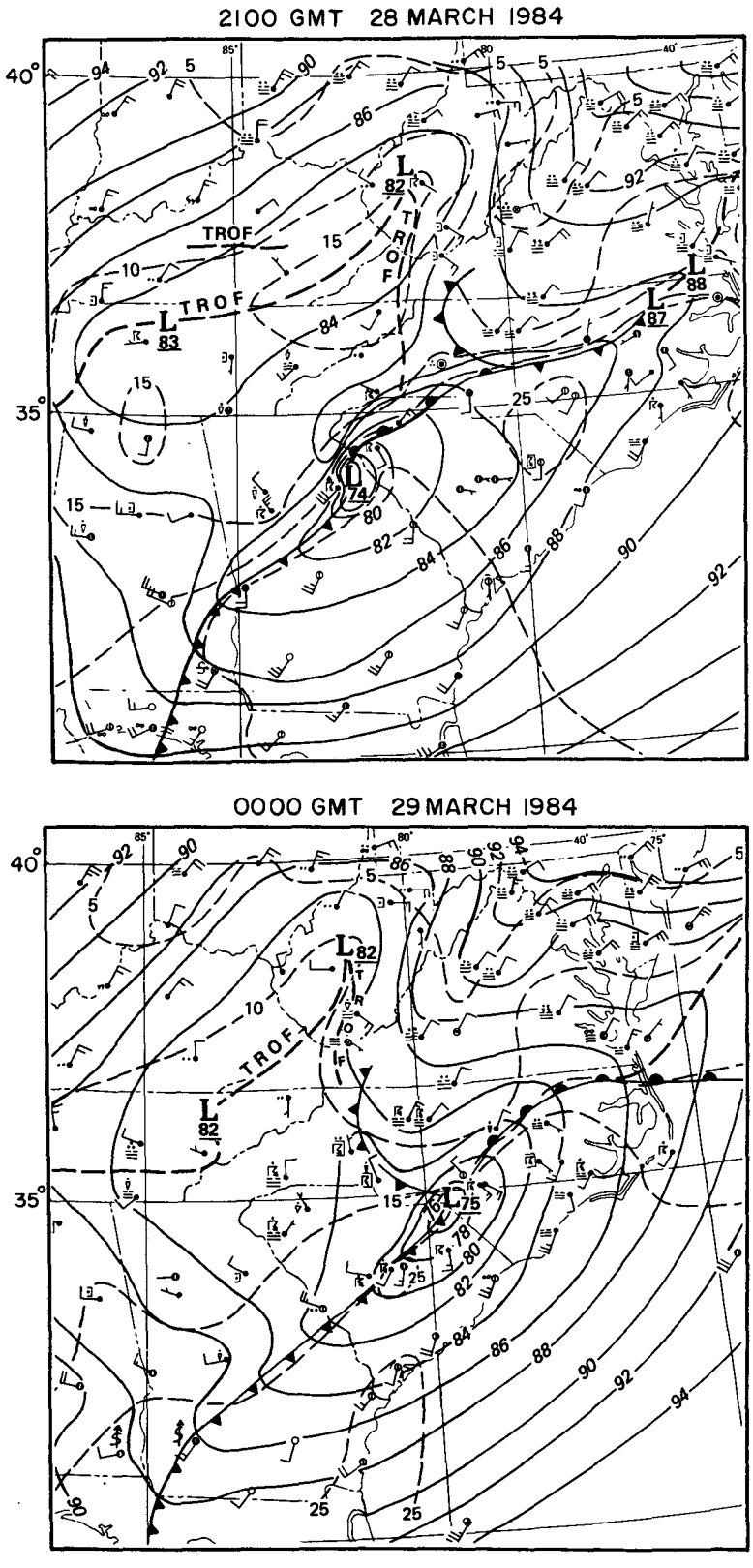

FIG. 8. (*Continued*)

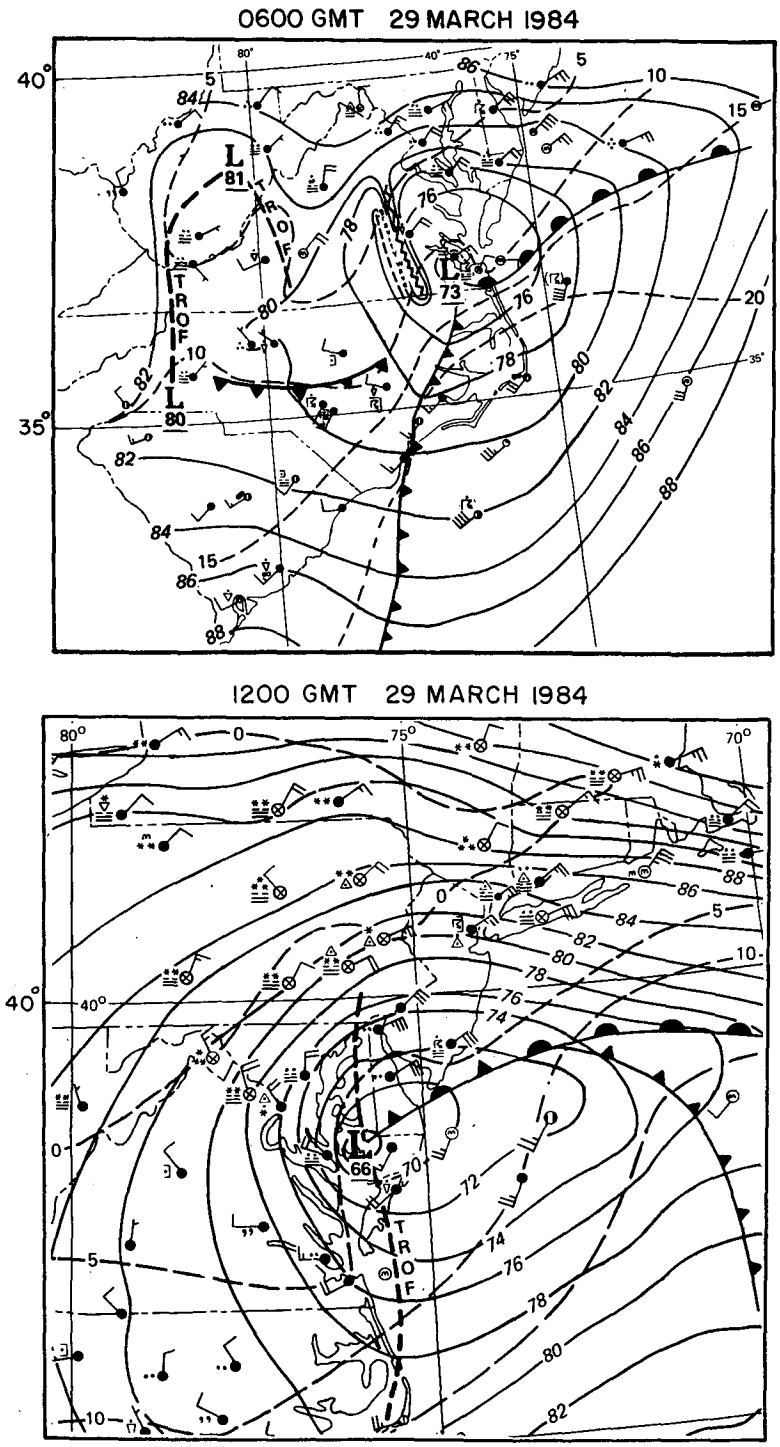

FIG. 8. (*Continued*)

3. Observations of the mesoscale cyclogenesis

We begin this section by presenting sectional analyses (Fig. 8), manually constructed, of all available surface observations. These observations are also used in the diagnostic calculations shown in the next section. At 1200 UTC 28 March, the surface cold front through Mississippi is associated with convection. A clear area

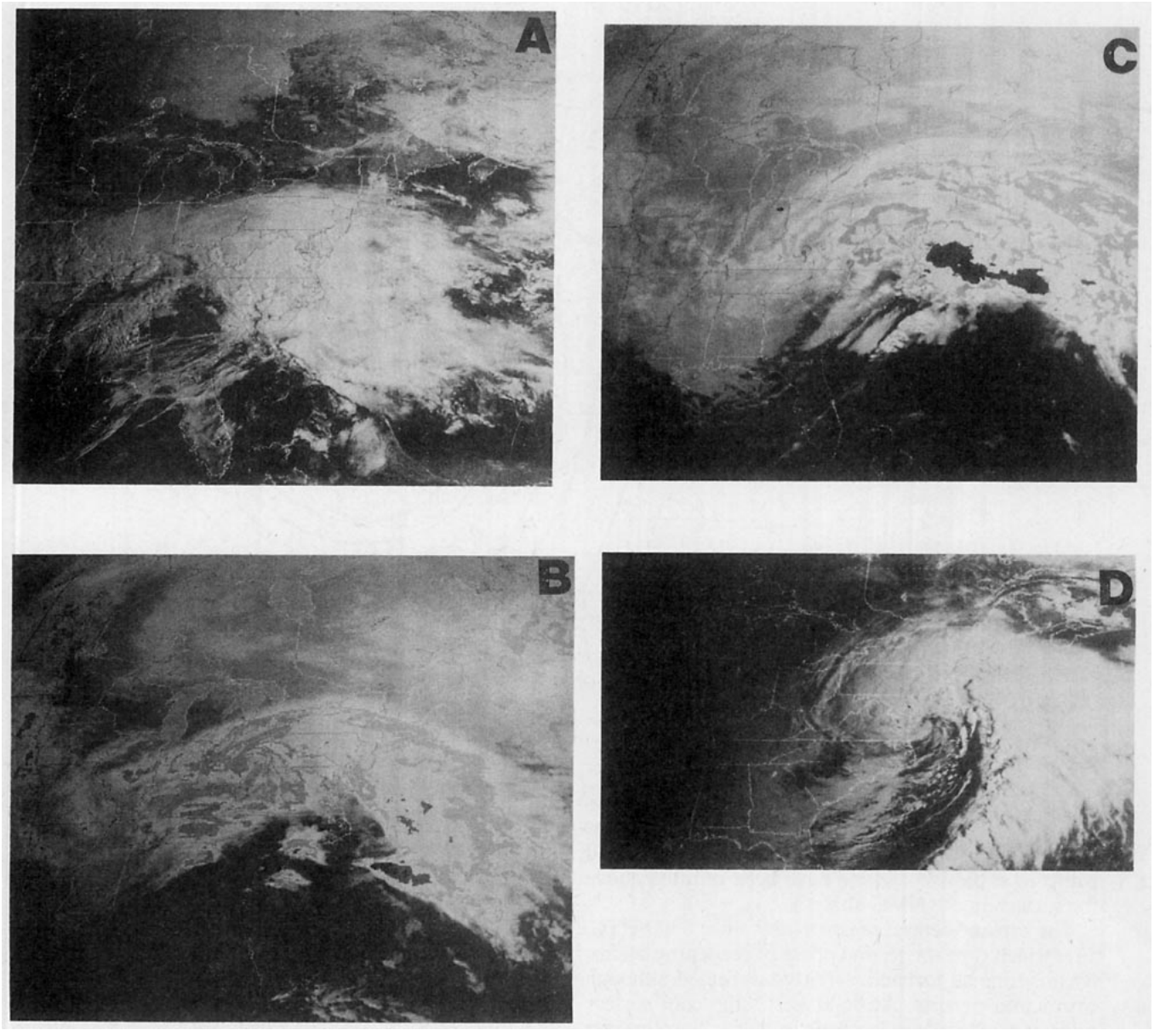

FIG. 9. Satellite images for (a) 1330 UTC 28 March (visible), (b) 2000 UTC 28 March (infrared), (c) 0400 UTC 29 March (infrared), and (d) 1230 UTC 29 March 1984 (visible).

lies to the east in Alabama and Georgia, where strong solar heating will take place during the day. These features are seen in the 1330 UTC satellite image (Fig. 9a). By 1800 UTC 28 March the 985 mb surface low first appears along this intensifying frontal system just to the west of Anniston, Alabama. The surface low had deepened 11 mb to 974 mb by 2100 UTC and had moved 25 m s^{-1} to a location just northeast of Athens, Georgia. The 22-tornado outbreak commenced shortly after this time, beginning with sightings in extreme western South Carolina. The baroclinic zone continues to strengthen along the cold front and northeastward from the low as the warm, moist surface air to the south contrasts with the cool surface ridge extending from Maryland to north-central North Carolina.

The mesoscale cyclonic circulation associated with the 975-mb low at 0000 UTC 29 March, is also clearly shown at 850 mb (Fig. 10a). Crucial to this analysis is the 6 m s^{-1} north-northeast wind at Greensboro (GSO). Additionally, another mesoscale low in West Virginia is clearly defined by the Pittsburgh, Dayton, and Huntington (HTS) winds. However, the HTS westerly and the GSO northerly winds were ignored in the operational National Meteorological Center

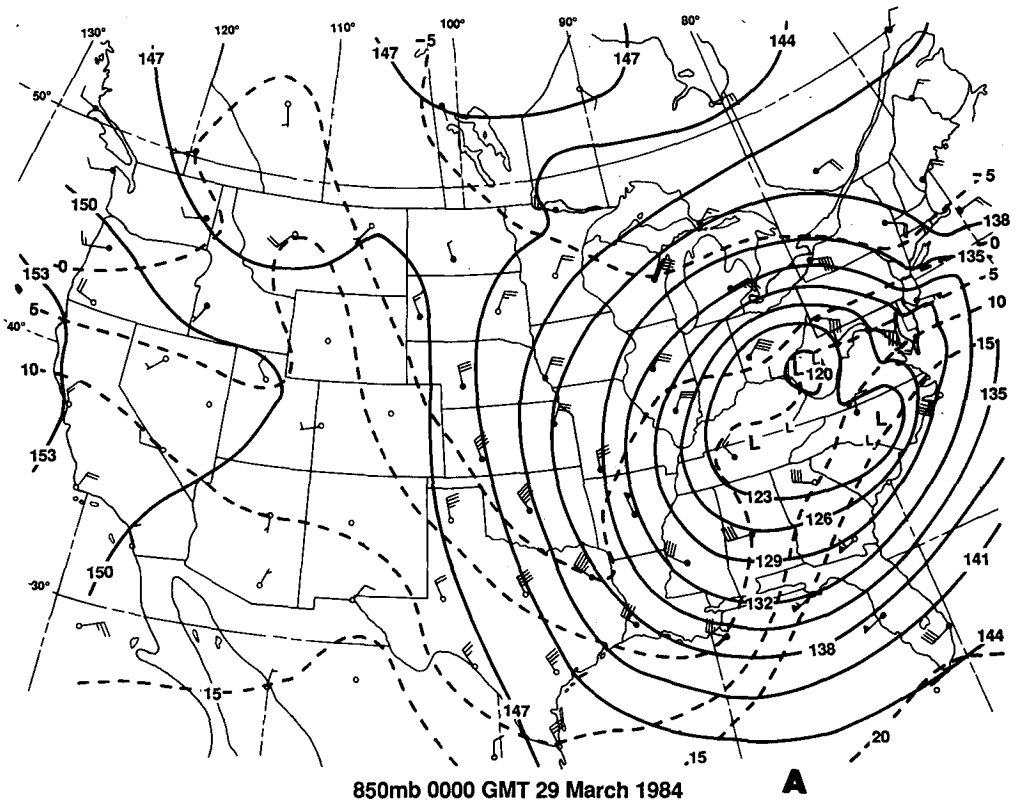

FIG. 10a. 850 height (solid, dam, contour interval of 3 dam) analysis and temperature (dashed, °C, contour interval of 5°C). Station plotting convention is as in Fig. 4. Smaller L's show surface cyclone positions.

(NMC) analysis (Fig. 10b), so that only one large cyclone is analyzed at the Kentucky–Tennessee border. Consequently, all mesoscale characteristics associated with this explosive cyclone have been omitted above the surface in the NMC analysis.

The cyclone central pressure rises until 0300 UTC, after which time the second phase of deepening begins. By this time all tornadic activity has ceased although convection persists. At 0600 UTC, the cool surface ridge east of the Appalachians in North Carolina has disappeared in the wake of the cold frontal passage. The small-scale trough–ridge axes at 0600 UTC, separated by 30 km, represent a gravity wave with heavy precipitation and convection developing along the ridge axis. The low continues to deepen through 1200 UTC 29 March, and sustained surface winds east and north of the low center range from 15 to 20 m s^{-1}. Several areas of heavy precipitation are occurring away from the 966 mb low. Deep convection exists along the offshore cold front. Heavy convective activity is occurring north of the warm front. The heaviest nonconvective precipitation extends along the trough axis northward from the low. The strongest geostrophic winds are north and west of the cyclone. The associated strong cold advection wraps around the cyclone in a spiral pattern. Similar processes were noted by Bosart (1981) in the Presidents' Day cyclone. The surface low at 1230 UTC is seen in the visible satellite image (Fig. 9d) with clouds wrapping around into the center. The deep convective cells are located offshore along both the warm and cold fronts.

To examine the relationship between the surface low center and precipitation, we present a series of radar Plan-Position Indicator (PPI) films in Fig. 11. The low at 1800 UTC 28 March is forming on the western edge of a thunderstorm complex which will spawn the bulk of the tornadoes in the Carolinas. From just after 1900 UTC through 2300 UTC 28 March, the low pressure system is nearly collocated with this tornadic thunderstorm complex. Echo intensities in excess of VIP 5 are indicated within 10 km of the surface cyclone center from 2000 through 2200 UTC. Echo tops at these times were at and above the tropopause level of about 15 km. These cold cloud tops over the surface cyclone in north-central Georgia are seen in the 2000 UTC satellite image (Fig. 9b). The first tornadoes originating from this convective complex occurred at 2220 UTC in South Carolina as the maximum echo tops were collapsing. As indicated in Fig. 2, the first period of intense cyclogenetic deepening occurs from 1800 through 2200 UTC 28 March, corresponding to the time interval in which the surface low is located within

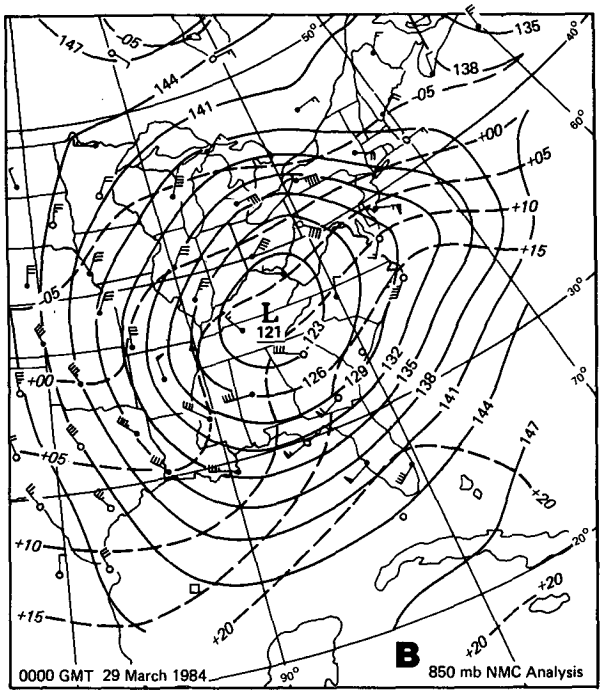

FIG. 10b. The NMC 850 mb height and temperature analysis for 0000 UTC 29 March 1984. Analysis and plotting convention as in (a), except that surface lows are not shown.

10 km of the significant convection. Tracton (1973) has suggested that the bulk diabatic effects of cumulus convection may directly effect incipient cyclogenesis. Our results here certainly support that suggestion.

After 2300 UTC 28 March this filling low begins to disassociate itself from the intense convection of the tornadic supercell. The only further close association between the low and convection occurs at 0600 UTC 29 March when the cyclone was located along a line of VIP-3 echoes (not shown). This is a time during which the low was deepening. However, we could find no other hours during this second pulse of deepening in which the convection and the surface low were nearly collocated. We suspect that the low's second phase of development was due more exclusively to synoptic-scale processes. This topic will be addressed in the concluding discussion. Figure 8 shows that several surface lows, spaced approximately 300 km apart, exist at 1800 UTC 28 March, the beginning of the first deepening. By 0600 UTC 29 March, the surface low was the dominant center of a cyclonic circulation extending over 1000 km in all directions.

4. Frontogenetic forcing

We evaluate surface frontogenetic forcing in the vicinity of the developing surface low using observed wind and thermodynamic fields objectively analyzed to a one degree latitude–longitude grid in the same way as described in section 2. The expression, for the time change of the magnitude of the virtual potential temperature gradient, following Petterssen (1956), is

$$\frac{d}{dt}|\nabla\theta| = \frac{1}{2}|\nabla\theta|\left[\left(\frac{\partial u}{\partial x} - \frac{\partial v}{\partial y}\right)\sec 2a \cos 2b - \nabla\cdot\mathbf{V}_h\right] \tag{2a}$$

where a is the angle between the dilatation and x axes, b is the angle between the potential temperature isotherms and dilatation axes, $\mathbf{V}_h$ is the horizontal wind vector, and the rest of the symbols are defined in the Appendix. We use this formulation to determine the effect the observed surface wind field has in changing the magnitude of an existing potential temperature gradient. We also use this formulation to determine the role of the surface geostrophic wind in changing the potential temperature gradient magnitude. Additionally, we may assess the direct role of differential diabatic temperature changes at the surface in changing the magnitude of the horizontal temperature gradient. This expression is

$$\frac{d}{dt}|\nabla\theta| = \nabla\frac{d\theta}{dt}. \tag{2b}$$

The results of the observed surface wind calculations [Eq. (2a)] are displayed in Fig. 12. At 1800 UTC 28 March, strong frontogenesis exists in central North Carolina at the southern boundary of the cool surface ridge (Fig. 8). The low forms along a second axis of strong frontogenesis through Alabama (see arrow). By 2100 UTC, the maximum frontogenetic forcing has nearly doubled since 1800 UTC, and its axis is closely aligned with the surface cold front. This intense frontogenesis occurs concurrently with the explosive cyclogenesis. At 0000 UTC 29 March, the main area of frontogenesis has merged with the southern boundary of the cool surface ridge. The maximum value of frontogenetic forcing, located nearly at the cyclone's center, has remained essentially constant during the previous three hours, as has the cyclone central pressure. By 0600 UTC, a significant change has taken place in that the intensifying cyclone is now located well to the west of the most intense frontogenetic forcing. Indeed, the 0400 UTC infrared image (Fig. 9c) shows the enhanced area of high cloud to the east of the surface low, offshore of Virginia and North Carolina, in this area of frontogenesis. The primary frontogenetic forcing at both 0600 and 1200 UTC 29 March exists to the northeast of the low. Heavy precipitation, in the form of thundershowers (Fig. 8), is occurring along this warm frontal axis.

To understand the contribution of the surface frontogenesis by the geostrophic flow, we have computed (2) using the geostrophic winds, and the resulting di-

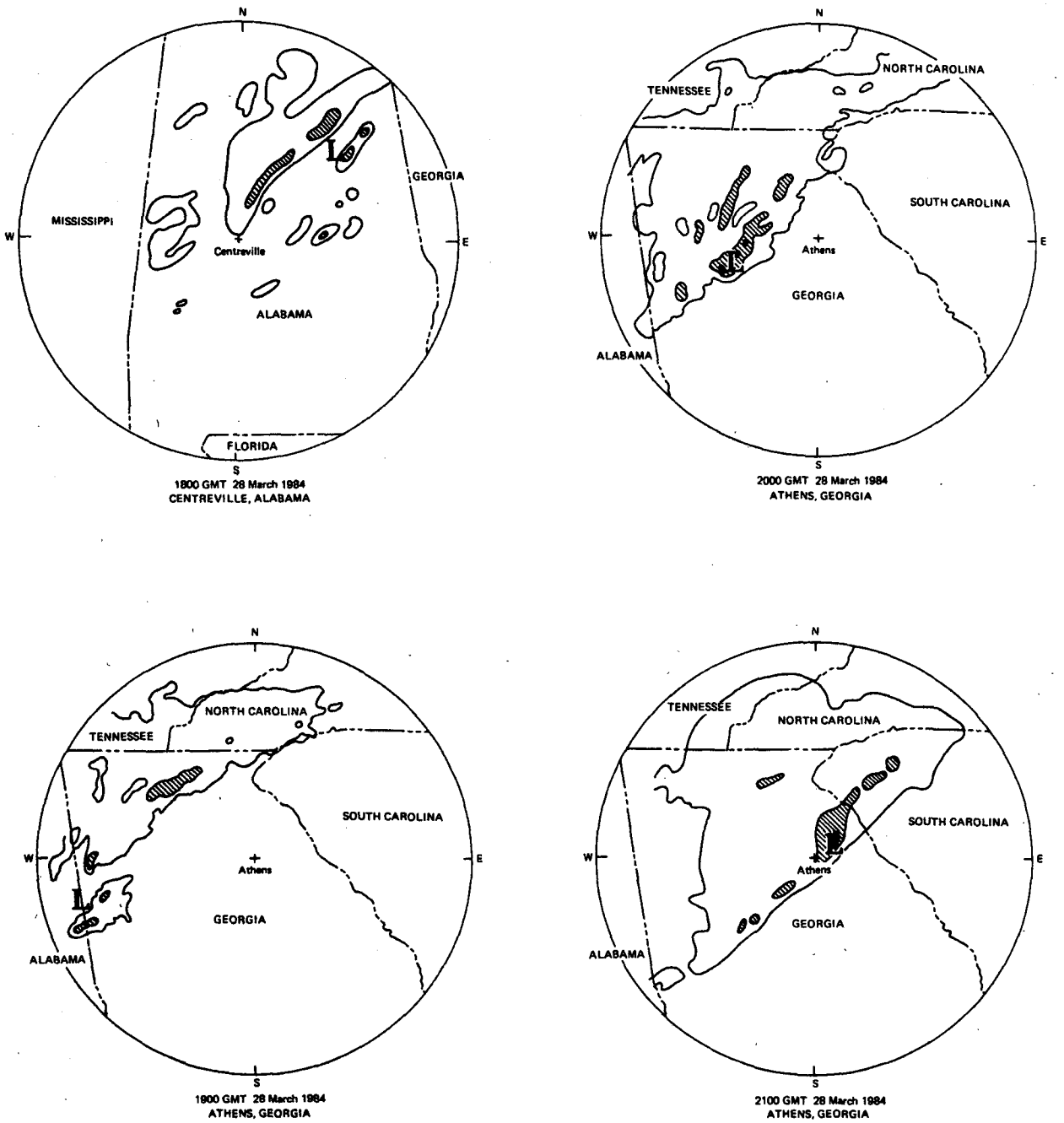

FIG. 11. Plan-Position Indicator (PPI) WSR-57 radar films showing hourly precipitation echoes, from 1800 UTC 28 March through 0100 UTC 29 March. VIP-level 1 threshold is outlined. Shaded regions enclose areas with at least VIP-level 3 echoes and double shading encloses echoes of VIP-5 or greater. Dots show small areas of VIP-3 or VIP-5 echoes, as appropriate. Radar sites are indicated at the center of each PPI. The 230-km radius circle surrounding the site is shown.

latation axes. These results are shown in Fig. 13. The geostrophic frontogenesis pattern through Alabama and the incipient cyclone at 1800 UTC 28 March closely resembles the frontogenesis due to the observed wind. The maximum geostrophic frontogenesis accounts for more than 40% of the observed wind maximum frontogenesis. By 2100 UTC, there is only a slight frontogenetic signal through the surface cyclone as compared with the observed wind frontogenesis. The geostrophic pattern is mainly frontolytic at 0000 UTC 29 March where most of the actual frontogenetic forcing is occurring through the intense surface cyclone.

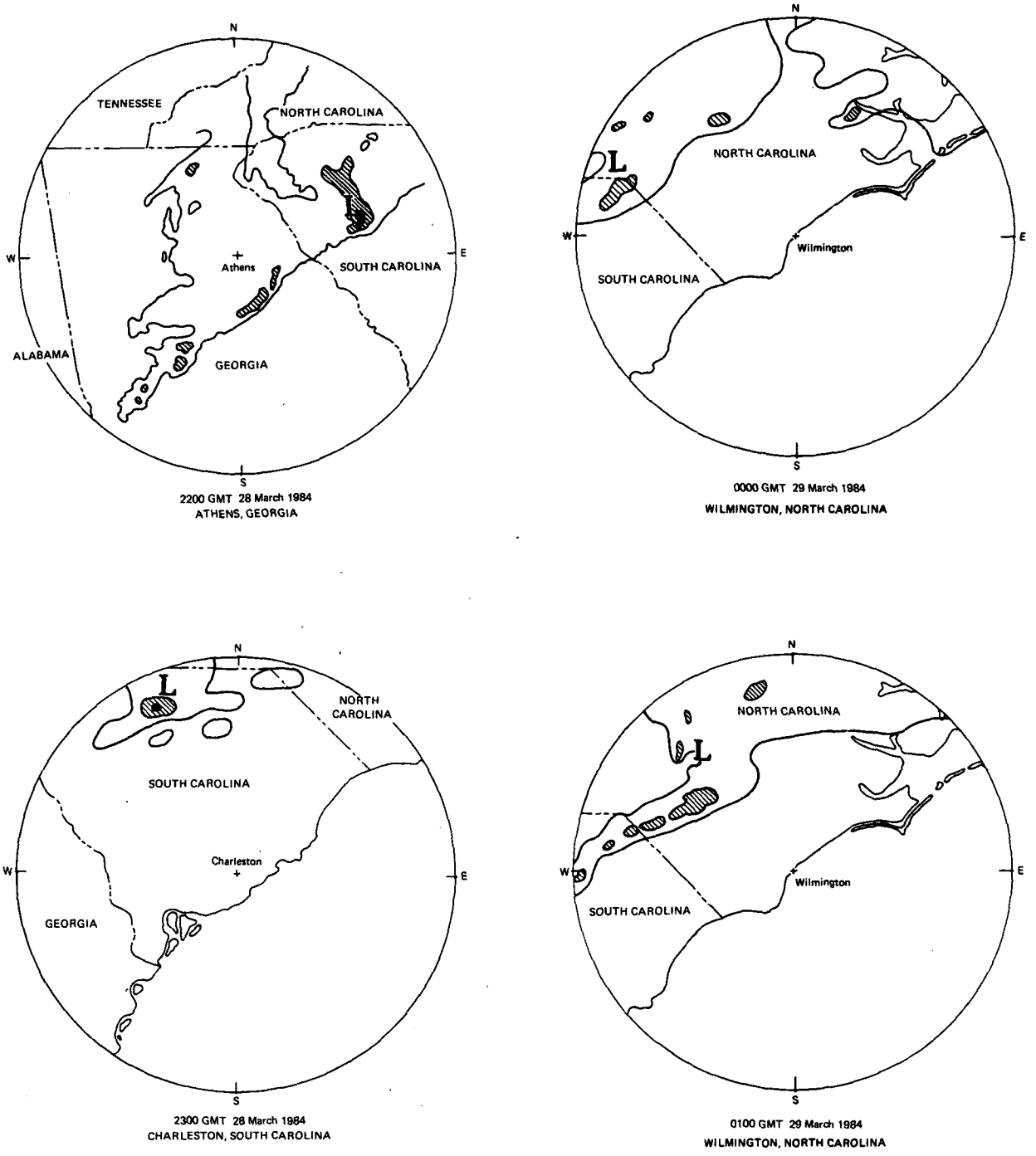

FIG. 11. (*Continued*)

This same sign difference in the calculations persists through 1200 UTC 29 March.

Figure 14 shows the hourly evolution of both maximum geostrophic and observed wind frontogenesis along the developing cold front. These results show quite clearly that the horizontal wind frontogenesis process, although weak compared with later times, helps initiate the surface baroclinic zone along which the cyclone forms, and is predominately geostrophic prior to 1800 UTC. However, once the front becomes strong, at 1800 UTC, the continued frontogenetic process is controlled by the ageostrophic flow. The transition from important geostrophic to ageostrophic frontogenesis occurs mainly during the initial 3-h pe-

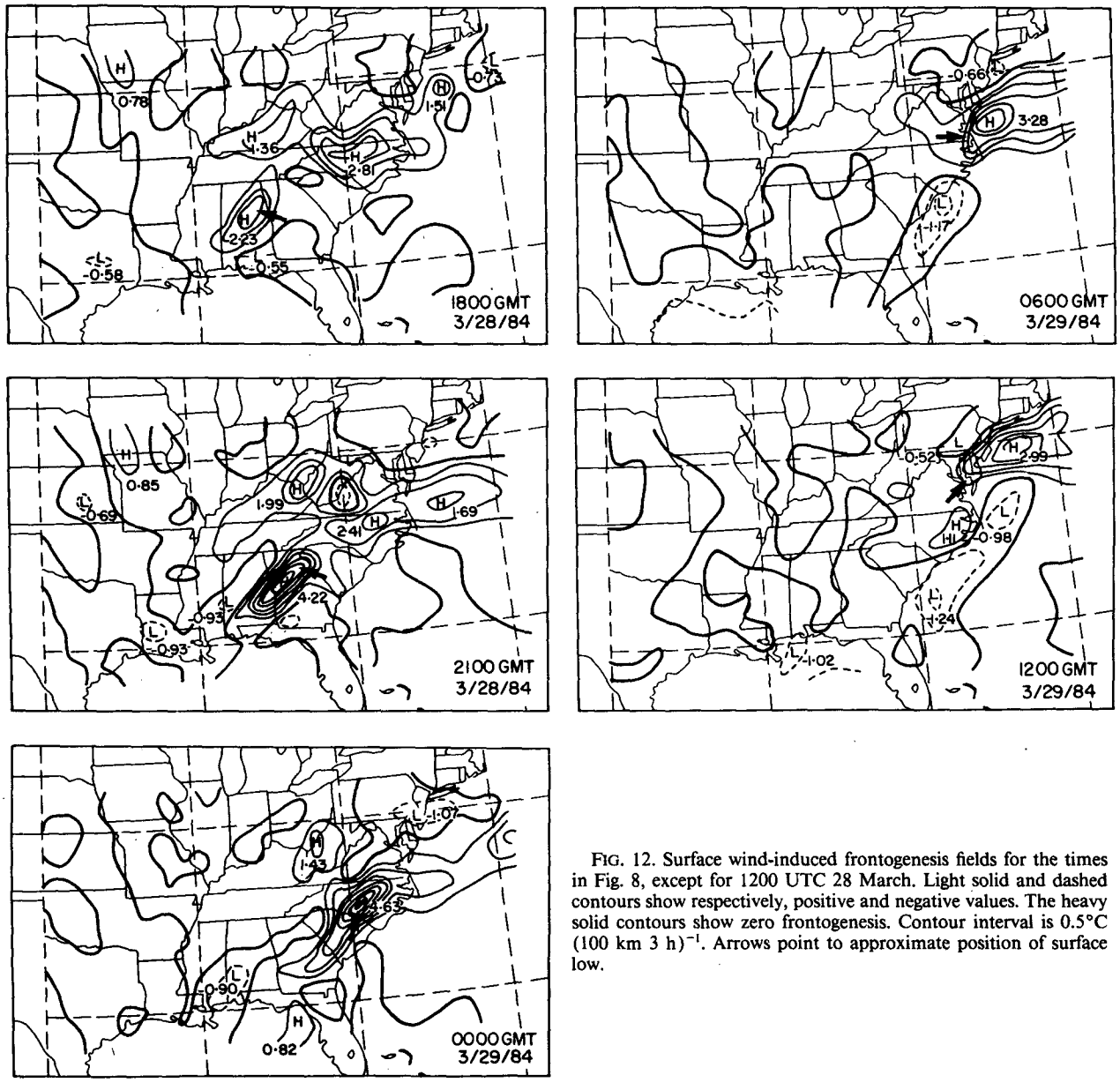

FIG. 12. Surface wind-induced frontogenesis fields for the times in Fig. 8, except for 1200 UTC 28 March. Light solid and dashed contours show respectively, positive and negative values. The heavy solid contours show zero frontogenesis. Contour interval is 0.5°C (100 km 3 h)$^{-1}$. Arrows point to approximate position of surface low.

riod of explosive cyclogenesis beginning at 1800 UTC 28 March. This transition process has been discussed theoretically by Hoskins (1982). Evidently, the continued role of ageostrophic flow is to enhance the baroclinity within which the surface cyclone continues to grow.

To understand the direct diabatic component of the surface frontogenetic forcing, we have utilized our objectively analyzed wind and temperature fields to compute hourly local potential temperature changes ($\partial\theta/\partial t$) and horizontal advection of potential temperatures. The residual component of temperature change is ascribed to diabatic heating in the expression

$$\frac{\partial\theta}{\partial t} = -\mathbf{V}_h \cdot \nabla\theta + \frac{d\theta}{dt}. \tag{3}$$

Two consecutive hours of instantaneous advective temperature changes are averaged to find the hourly advective temperature change. The results are shown in Fig. 15. The differential diabatic heating that occurs across the front is strong. The diabatic warming in the warm air of eastern Mississippi between 1100 and 1200 UTC moves eastward and intensifies with increases in excess of 3°C seen in the warm air of southern Alabama between 1500 and 1600 UTC. This pocket of diabatic warming is located to the southeast of the developing

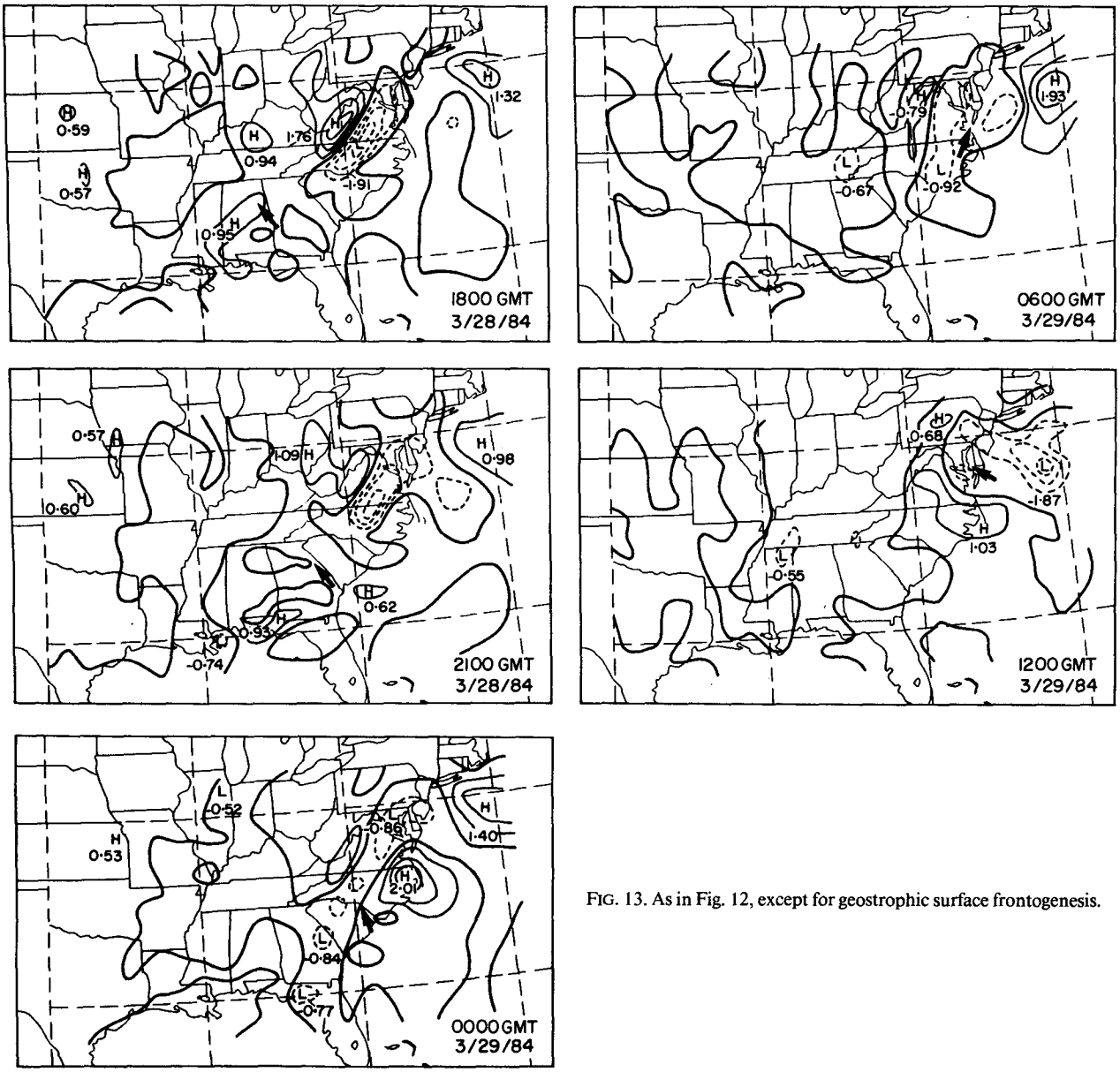

FIG. 13. As in Fig. 12, except for geostrophic surface frontogenesis.

cold front. The two centers of maximum diabatic heating seen between 1300 and 1400 UTC 28 March in the extreme western Carolinas and southwestern Alabama are seen dramatically by clear areas in the 1330 UTC visible satellite image (Fig. 9a).

In order to quantitatively assess the frontogenetical effect of the surface diabatic processes, we have computed the difference between the diabatic temperature changes at points 100 km to the warm side of the cold front, and 100 km to the cold side. These two points define a line segment oriented normal to the isotherm located at the point along the front at which the maximum observed wind frontogenesis is found. These results from Eq. (2b), along with the geostrophic and observed horizontal deformation calculations from Eq. (2a), are shown in Fig. 14. It should be emphasized that convectively driven diabatic effects are implicitly present in the observed surface wind-induced frontogenesis (Eq. 2a) by way of the ageostrophic wind contribution associated with convective ascent. Clearly the diabatic effects associated with strong boundary layer heating in the warm air intensified the horizontal temperature gradient well before the appearance of the cyclone at 1800 UTC 28 March. Additionally, a substantial contribution to the frontogenesis comes from horizontal deformation, with the geostrophic flow ac-

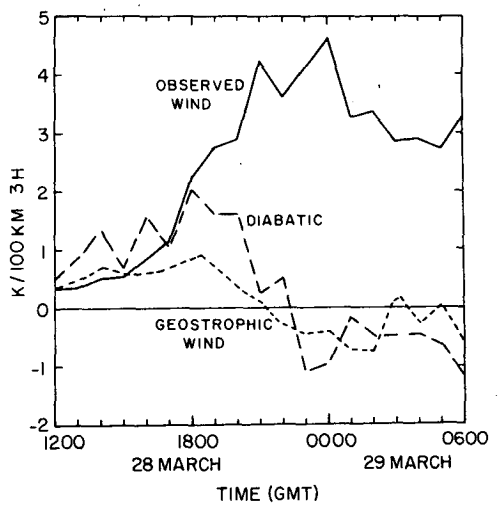

FIG. 14. Time series of diabatic (dashed), geostrophic wind (short dashed), and observed wind (solid) frontogenetic forcing computed at the points of maximum observed wind frontogenesis along the developing cold front (°C/100 km 3 h).

counting for a substantial portion prior to the cyclogenesis. Thus, geostrophic flow and differential diabatic heating act together to intensify the baroclinic zone along which the mesocyclone forms, several hours *prior* to cyclogenesis. The satellite imagery and radar data show a close relationship between the dominant surface frontogenesis areas and precipitation. As an example, the line of strong surface frontogenesis at 2100 UTC extending from western South Carolina southwestward through northern Georgia and southeastern Alabama (Fig. 12) corresponds closely to the organized line of convection (Fig. 11) for the same time. This same line is seen in the 2000 UTC satellite imagery (Fig. 9b). Additionally, the offshore warm frontogenesis region, appearing at 0600 UTC 29 March in Fig. 12, corresponds closely to the deep and high cloud band with heavy precipitation, offshore of Virginia, in Fig. 9c.

5. Soundings, static stability, and potential vorticity

The thermodynamic sounding for Centreville, Alabama, at 1200 UTC 28 March (Fig. 16a), representative of the environment surrounding the incipient cyclogenesis, shows several layers of deep conditional instability above the morning surface inversion. The atmosphere, though mainly unsaturated, has some pockets of nearly saturated low-level air. The moist inversion below 700 mb and the strong wind shift between 750 and 700 mb denote a frontal zone whose surface counterpart is in the southern part of the state (Fig. 4a). The nearly moist adiabatic lapse rate is probably a result of the convection occurring in the area prior to 1200 UTC. The tropopause height of 138 mb is suggestive of a tropical sounding. Given this sounding's weak stability and high moisture content, it is not surprising that more convection broke out in this area, after surface temperatures had risen to 21°C at the station, and to 27°C at Montgomery, Alabama, located 100 km to the southeast.

The Greensboro sounding at 0000 UTC 29 March (Fig. 16b), north of the surface cyclone, clearly shows a deep moist layer extending nearly uninterrupted from the surface to above 500 mb. The strong static stability seen between 880 and 930 mb is the upper boundary of the cool surface air dammed against the Appalachians. Above this layer, the layers are either conditionally unstable or neutral through 500 mb. Convec-

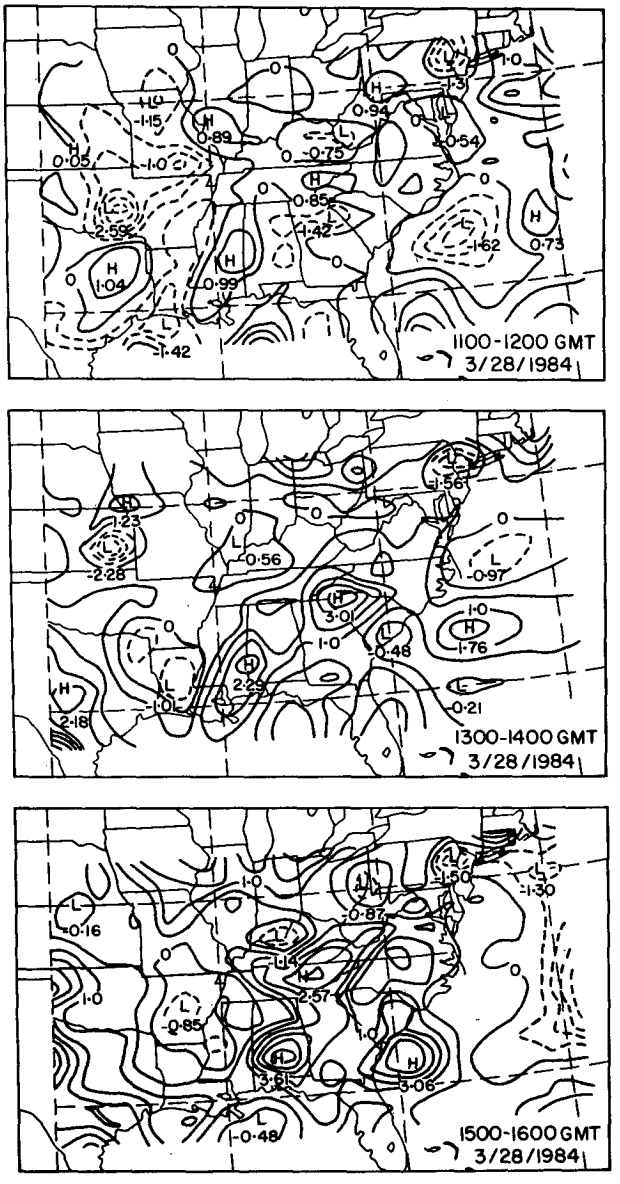

FIG. 15. Hourly diabatic temperature changes (°C) for the time periods shown. Contour interval is 0.5°C. Dashed lines indicate cooling.

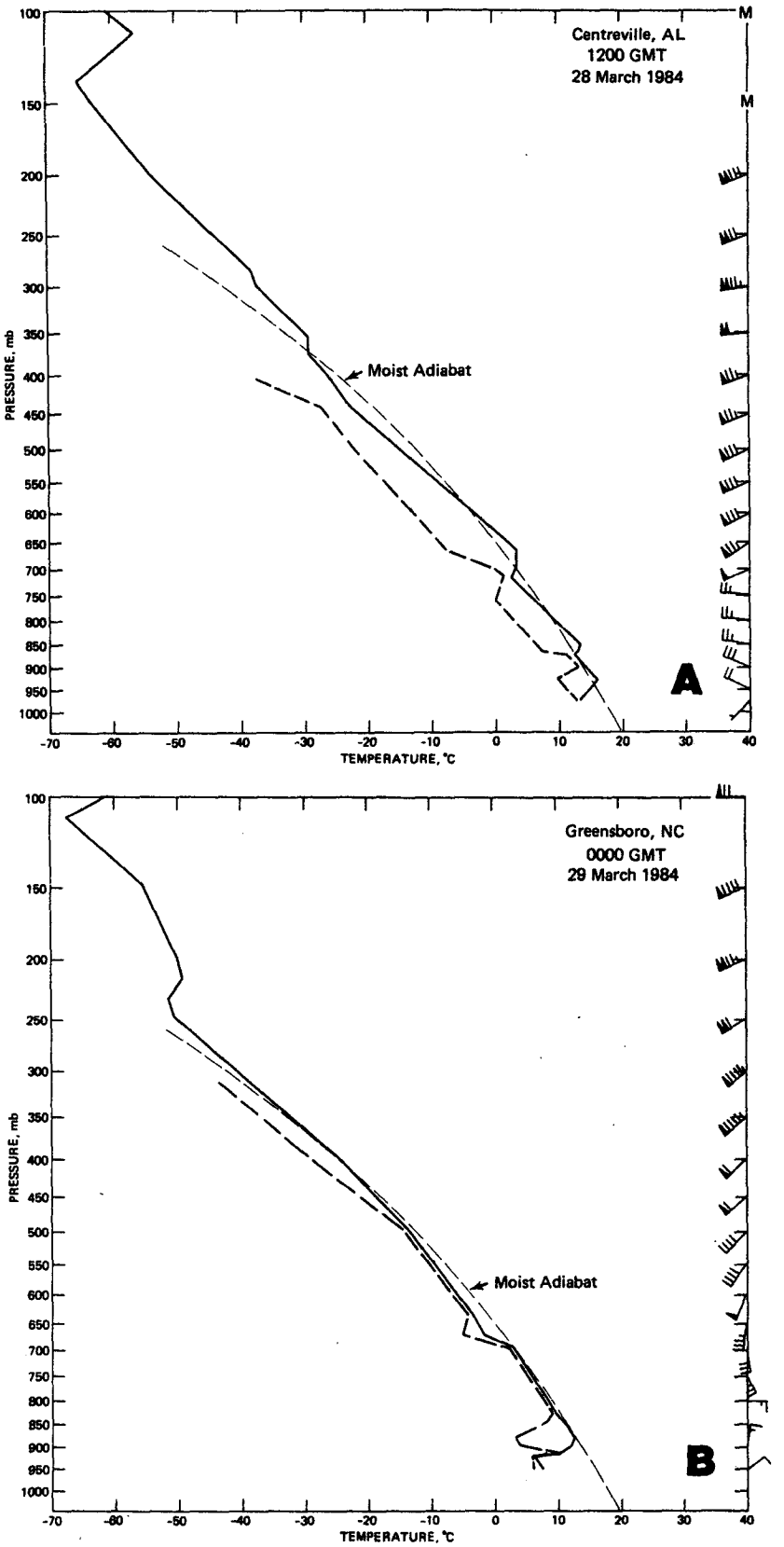

FIG. 16. Soundings for (a) Centreville, Alabama, at 1200 UTC 28 March 1984 and (b) Greensboro, North Carolina, at 0000 UTC 29 March 1984. Temperatures and dewpoints are shown by the heavy solid and heavy dashed lines, respectively. The moist adiabats are indicated by light dashed lines. Winds are plotted in the same manner as for Fig. 4.

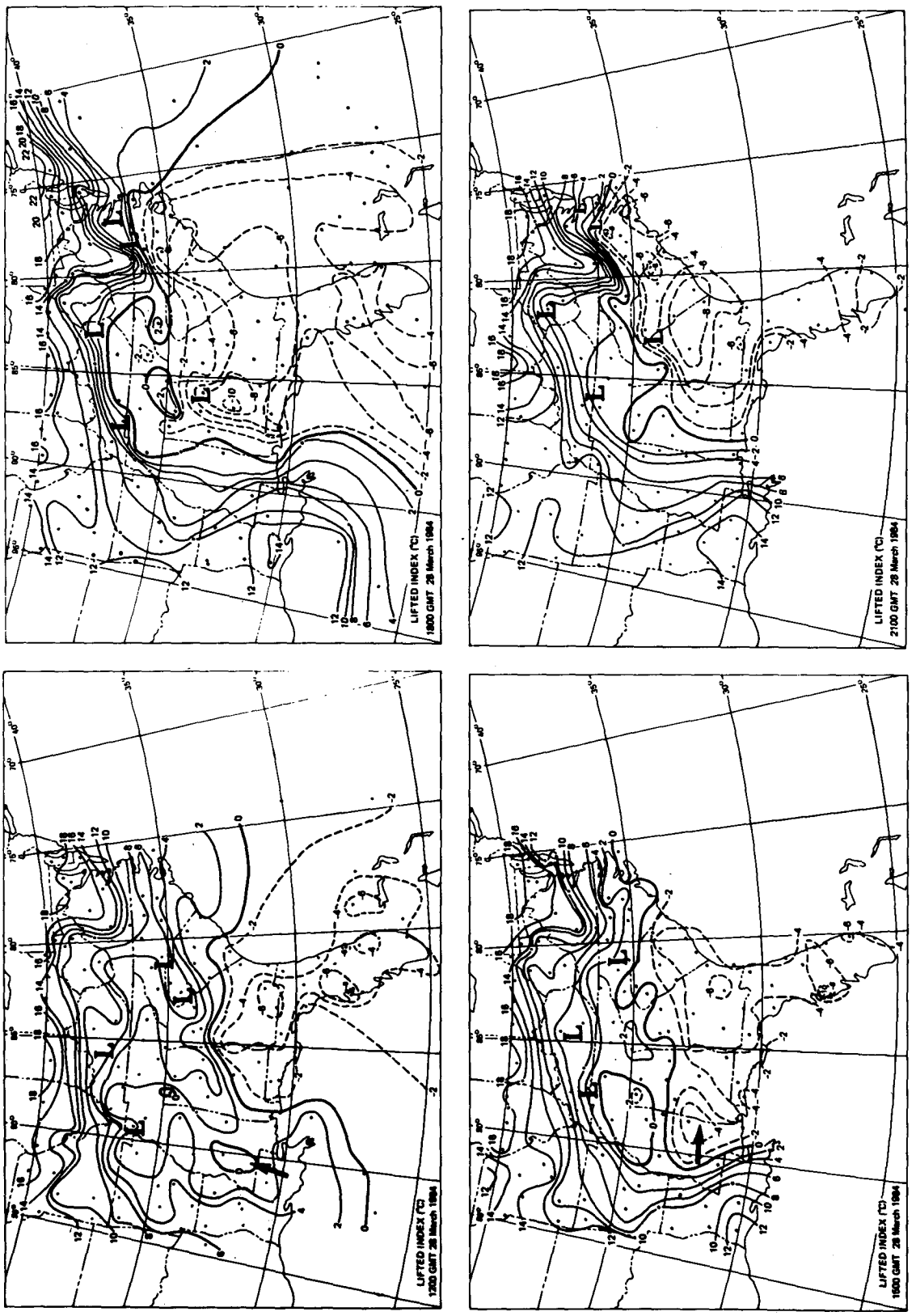

FIG. 17. Lifted index (°C) analysis for 1200, 1500, 1800 and 2100 UTC 28 March 1984 and for 0000, 0300 and 0600 UTC 29 March 1984. Contour interval is 2°C, with negative values dashed. Surface data points are encircled. Surface low positions are indicated with an "L". Arrows in the first two frames point to areas discussed in the text.

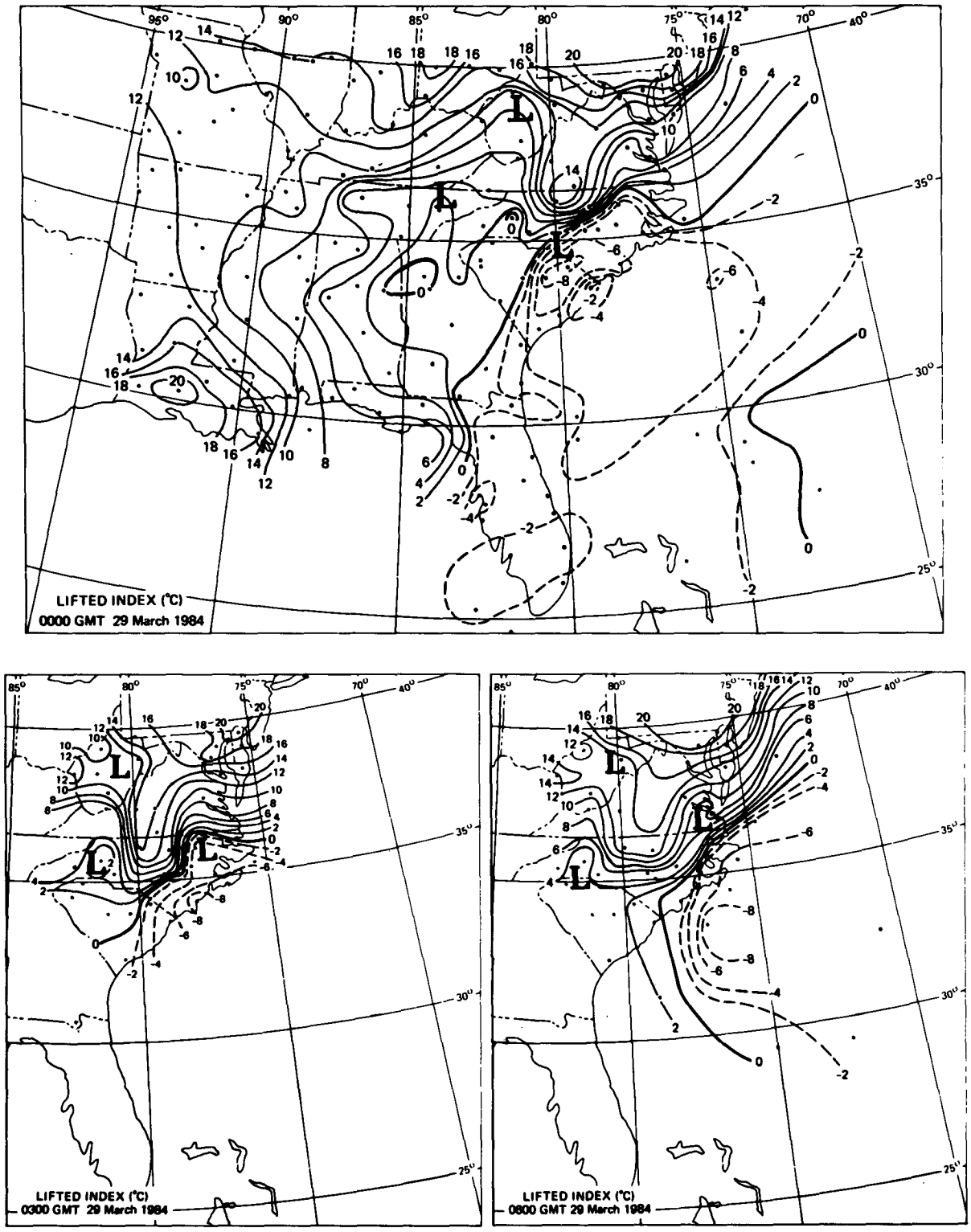

FIG. 17. (*Continued*)

tion is observed at the time and location of the sounding, approximately 100 km to the north of the surface low (Fig. 8). Substantial veering of the wind is seen above the lowest stable layer to 500 mb, which shows warm advection. This warm advection, helping to force the large-scale ascent seen in the region (Fig. 7), provides a favorable environment for the convection.

So that we may assess static stability changes more frequently than every 12 h, we have utilized the dense array of surface data (station elevation, pressure, temperature, and dew point) to compute lifted indices. We define the lifted index as the difference between the 500-mb environmental temperature and the 500-mb lifted surface parcel temperature. A linear time interpolation of the 500-mb temperature analysis was performed at each surface location for the nonsynoptic times. These analyses are shown in Fig. 17. At 1200 UTC 28 March, the intensifying cold front lies along an axis of weak stability in southwestern Mississippi (see arrow) with lifted indices below 0°C. By 1500 UTC, this area shifts eastward to the Alabama–Mississippi border and destabilizes. The destabilization continues as this unstable area moves into east-central Alabama at 1800 UTC. The Montgomery, Alabama, surface report yields a −11°C lifted index for this time. The intersection of the surface cold front and the axis of maximum instability is the point at which the surface low pressure system develops. The area of unusually low lifted indices (≤ -5°C) extends eastward of the developing low center to the Atlantic Coast. Thus, the low center subsequently moves eastward into an area of strong static instability. The surface low continues to be surrounded by unstable air until 0300 UTC 29 March, when the low lies on the unstable side of a strong stability gradient. The strongly stable surface air at the Virginia–North Carolina border lies in the midst of the cool surface ridge seen in Fig. 8. However, above this stable surface layer, the air is likely much less stable, or even conditionally unstable, as suggested by the Greensboro sounding (Fig. 16b). By 0600 UTC 29 March, the surface low lies in the midst of stable surface air, even though intensification has resumed (Fig. 2).

In summary, this potential instability (as defined by the lifted index) grew *prior* to the initial cyclogenesis at 1800 UTC 28 March. At this time, the combination of surface frontogenetic forcing (Fig. 12) and enhanced instability was maximized where the low formed. We speculate that the low-level convergence associated with the rising branch of the thermally-direct circulation, a response to the frontogenetic forcing (Sawyer 1956), was maximized where the static stability was the weakest. This maximum convergence would have contributed to enhanced vorticity generation at the point of the surface low's development. An examination of the 1200 UTC 28 March and 0000 UTC 29 March quasi-geostrophic analyses (Fig. 7) suggests that substantial ascent would exist over the developing surface low at 1800 UTC. This ascent allows the potential instability to be released, and convection to occur. This convection, while stabilizing the atmosphere toward neutrality, would dominate the larger scale motions. Once this stabilization has occurred, the mesoscale frontogenetic circulation, described above, would continue to aid the low's development.

The low's second phase of development, beginning at 0400 UTC 29 March, occurred in spite of its proximity to enhanced surface-based static stability. The larger scale of the low by this time (Fig. 8) suggests that the low's development would be less sensitive to static stability. This second phase of development will be discussed in section 7.

To consider the role of diabatic and frictional processes in this cyclogenesis, we have computed potential vorticity throughout the cyclone domain. Any change in the potential vorticity, S, of an air parcel would imply the importance of either or both friction and diabatic heating in this change, since S is conserved for frictionless and adiabatic motions (Ertel 1942). Thus for this conservation,

$$dS/dt = 0, \tag{4}$$

where $S = (\alpha \cdot \nabla_3 \eta)/\rho$, α is the absolute vorticity vector, η is the function of state, ∇_3 is the three-dimensional gradient operator, and ρ is the density. If the potential temperature θ is the function of state, the atmosphere is hydrostatic, and θ changes most rapidly in the vertical, Eq. (4) becomes

$$\frac{d}{dt}\left[-g(\partial\theta/\partial p)(\zeta_\theta + f)\right] = 0 \tag{5}$$

where g is gravity, f is the Coriolis parameter, and ζ_θ is the relative vorticity evaluated on a θ surface. We compute the static stabilities from our grid-point objective analysis of θ each 15 mb, and objective wind (u and v) analyses on θ surfaces each $2K$.

Cross sections of gravity-weighted potential vorticity through the developing cyclone center are shown in Fig. 18. The temporal increase in lower tropospheric potential vorticity directly over the cyclone center is clearly shown. By 0000 UTC 29 March, lower tropospheric potential vorticities over the surface cyclone exceed the stratospheric threshold of 1×10^{-5} K mb^{-1} s^{-1} (Reed and Danielson 1959). However, the atmosphere is nearly saturated where these large lower tropospheric potential vorticities exist. Therefore, this high potential vorticity air is fundamentally tropospheric, and we conclude that these high values of potential vorticity are generated in situ over the surface cyclone center. This apparent potential vorticity generation in other explosive cyclones has been discussed by Gyakum (1983b) for the *QEII* and Bosart and Lin (1984) for the Presidents' Day cyclone. The increase in the lower troposphere potential vorticity is related to a combi-

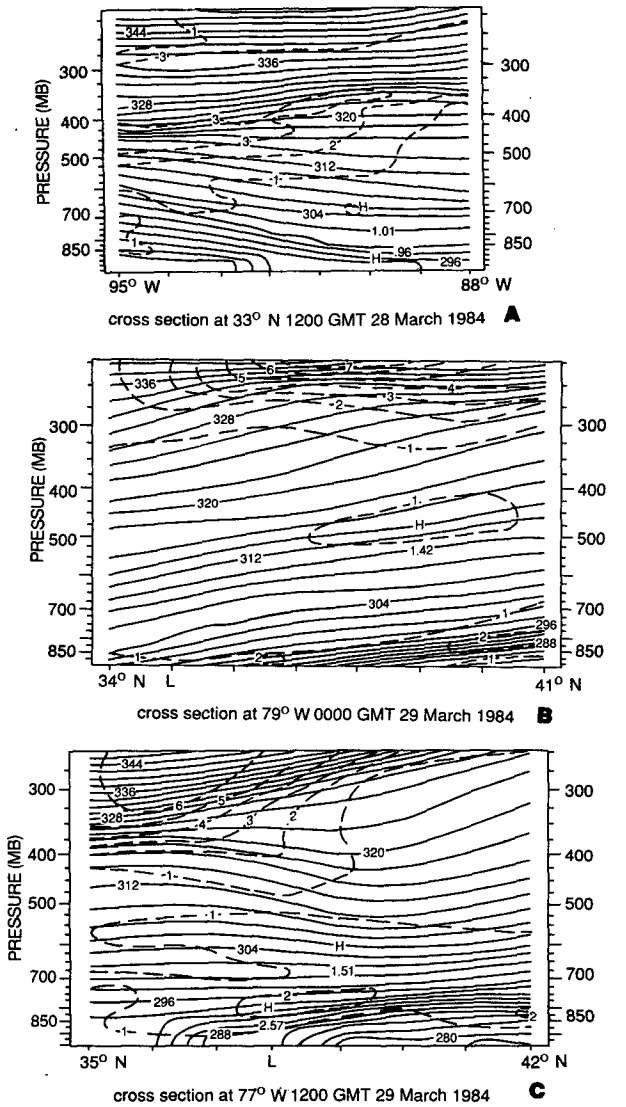

FIG. 18. Cross sections of potential temperature (solid, K), and potential vorticity $(-\partial\theta/\partial p)(\zeta_\theta + f)$ (dashed, 10^{-5} K mb^{-1} s^{-1}) along latitude 33°N (1200 UTC 28 March), longitude 79°W (0000 UTC 29 March), and longitude 77°W (1200 UTC 29 March). Low pressure system is indicated with an "L".

nation of static stability and absolute vorticity increases. The expression for the time rate of change of potential vorticity in the presence of friction and diabatic processes, as shown by Staley (1960) and Gidel and Shapiro (1979), among others, is

$$\frac{dS}{dt} = g\alpha \cdot \nabla_3 \dot{\theta} - g\left(\frac{\partial\theta}{\partial p}\right)\mathbf{k} \cdot \nabla_\theta \times \mathbf{F} \qquad (6)$$

where $\nabla_3\dot{\theta}$ is the three-dimensional gradient of diabatic temperature change, $\mathbf{k}$ is the vertical unit vector, ∇_θ is the gradient operator along a constant θ surface, and $\mathbf{F}$ is the frictional force per unit mass. As discussed in Gyakum (1983b), the diabatic heating term, resulting from vertical and horizontal variations in convection-induced temperature changes, can account for potential vorticity generations greater than what is found in this case. The frictional term, which involves horizontal variations in the vertical momentum flux divergence (Gyakum 1983b) may also be acting to produce potential vorticity in the vicinity of the convection. The intense cumulus convection, observed in the vicinity of this developing cyclone, and the associated latent heating, turbulent heat and momentum fluxes are prime candidates for these potential vorticity increases.

As a further check on the relationship between stratospheric air and the surface cyclone, we examined ozone concentrations for approximately 1800 UTC 28 and 29 March 1984 (Fig. 19). Large ozone concentrations are positively correlated with the stratospheric depth. Thus, high ozone content is associated with low tropopause heights. The instrument used is the Total Ozone Mapping Spectrometer (TOMS), which is flown aboard the Nimbus 7 polar-orbiting satellite and measures reflected ultraviolet radiation. Thus, measurements are made only once a day. Shapiro et al. (1982) provide details on the TOMS instrumentation, and have found TOMS to compare favorably with aircraft ozone measurements. The high values of ozone in Arkansas and northern Louisiana are related to the relatively low tropopause and high potential vorticity seen between 400 and 500 mb at 95°W in Fig. 18a at 1200 UTC 28 March. The high ozone values in excess of 400 Dobson units also correspond well with the 300 mb troughs (Figs. 4 and 5) and the associated cold thicknesses. By 1800 UTC 29 March a maximum of ozone exists directly over the surface cyclone center. This is associated with the 300 mb trough, along with the cold air (Fig. 6). Though this pattern of ozone looks similar to that found by Uccellini et al. (1985), we believe this collocation of an ozone maxima with the mature surface cyclone is a reflection of the cold, low tropopause upper-level trough being located directly above the surface low. Figure 18c shows stratospheric air penetrating to about 500 mb. However, as stated before, the separate potential vorticity maximum centered over the surface cyclone and between 700 and 800 mb has its origins in the troposphere. It is doubtful that high potential vorticity air descended into the lower troposphere; however, its movement into areas upstream of the surface cyclone likely aided the favorable environment for the cyclonic development.

6. Forecast implications

A sequence of 500 mb and sea-level pressure operational Limited-Area Fine-Mesh (LFM, see Gerrity 1977) forecast maps for the 24-h period beginning at 1200 UTC 28 March 1984 is shown in Figs. 20 through

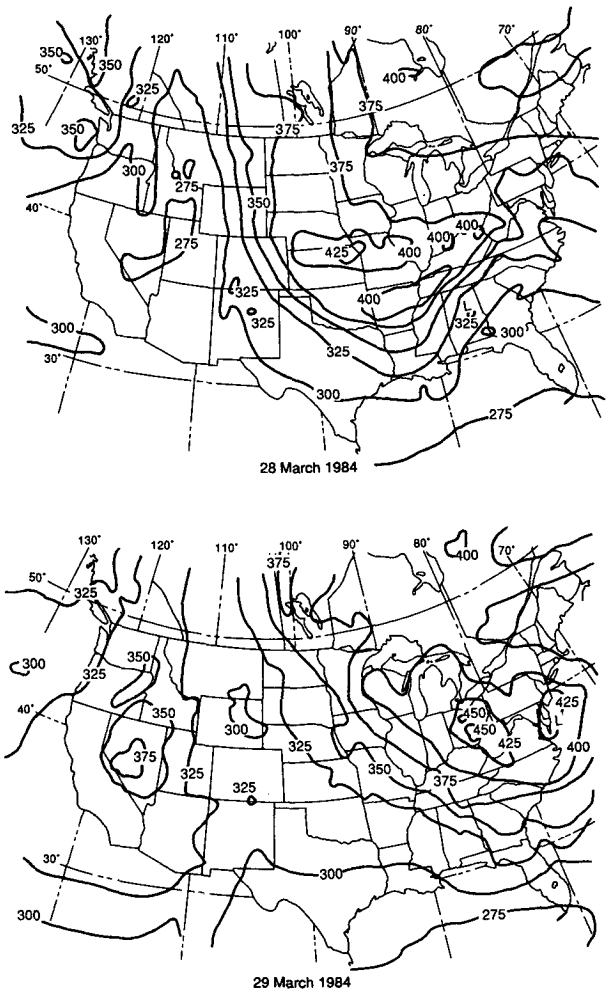

FIG. 19. Total ozone distribution, measured by the Total Ozone Mapping Spectrometer (TOMS) for 1800 UTC 28 and 29 March 1984. Dobson units are shown (1 DU = 10^{-3} atm-cm). Contour interval is 25 DU. Location of surface low for each time is shown by an "L".

22. At 1200 UTC 28 March (Fig. 20), the 985 cyclone in western Tennessee is well forecast, although the observed surface ridge (Fig. 4) extending from Maine southwestward into Virginia is absent from the forecast. The 500-mb cyclonic vorticity advection, over the developing cold front (Fig. 8) in Louisiana and Mississippi, is only weakly cyclonic in the 12-h forecast, whereas the analysis (not shown) indicates much stronger advection in this region. By 0000 UTC 29 March (Fig. 21), the 24-h forecast has completely missed the 975 mb mesoscale cyclone located along the North–South Carolina border (Fig. 5). Instead, the model erroneously continues to deepen the Tennessee cyclone seen at 1200 UTC 28 March and translates it into southwestern Virginia. A possible reason for this poor surface forecast was that 500 mb cyclonic vorticity advection, seen throughout the central and western Carolinas in the analysis (not shown), is virtually nonexistent in this 24-h forecast. At 1200 UTC 29 March (Fig. 22), the forecast 974 mb cyclone center compares

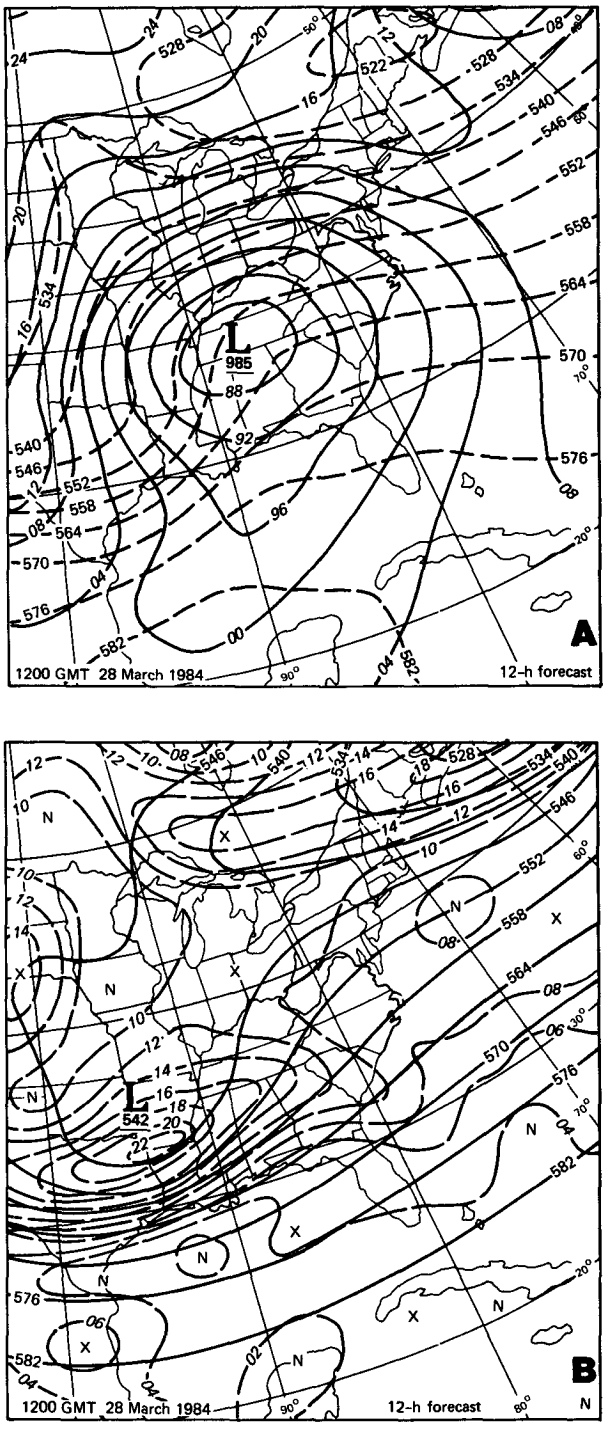

FIG. 20. LFM 12-h forecast of (a) sea-level pressure (solid, mb with hundreds and thousands digits omitted) and 1000–500 mb thickness (dashed, dam), and (b) 500 mb height (solid, dam) and absolute vorticity (dashed, 10^{-5} s^{-1}), for 1200 UTC 28 March 1984.

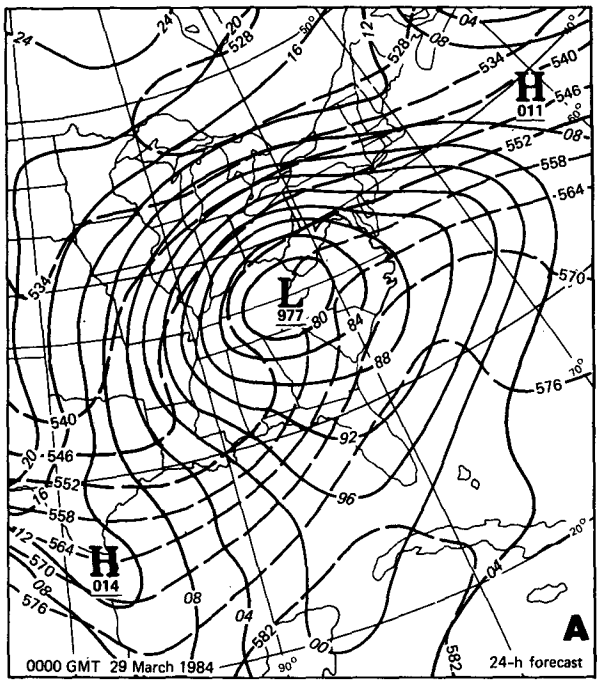

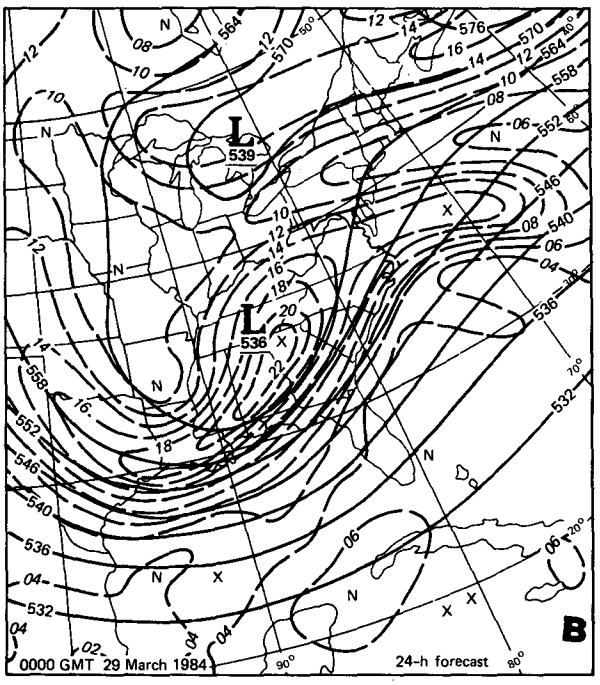

FIG. 21. As for Fig. 20, except for the 24-h forecast verifying at 0000 UTC 29 March 1984.

favorably with the LFM-analyzed 972 mb cyclone center. While the forecast and analyzed central pressures are similar, the model's Virginia cyclone (seen in Tennessee at 1200 UTC 28 March) has a completely different origin from the LFM-analyzed 972-mb cyclone located about 350 km farther to the east. Furthermore, the forecast 500 mb vorticity center in eastern North Carolina is actually found about 300 km to the northeast.

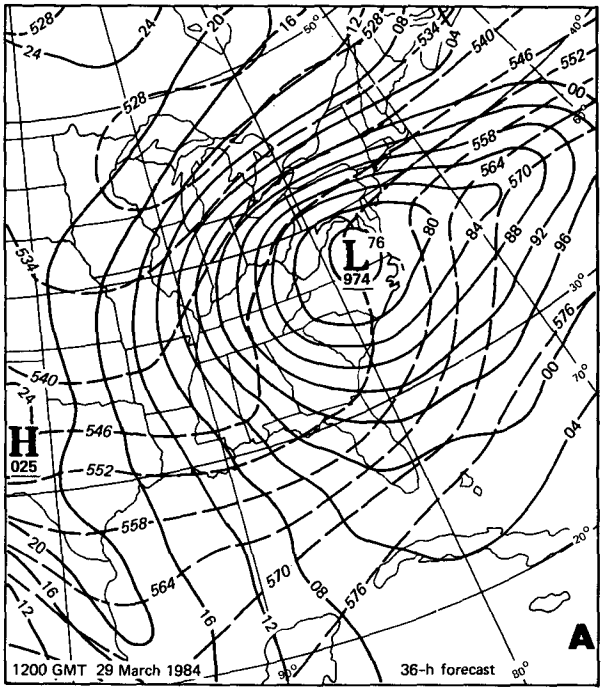

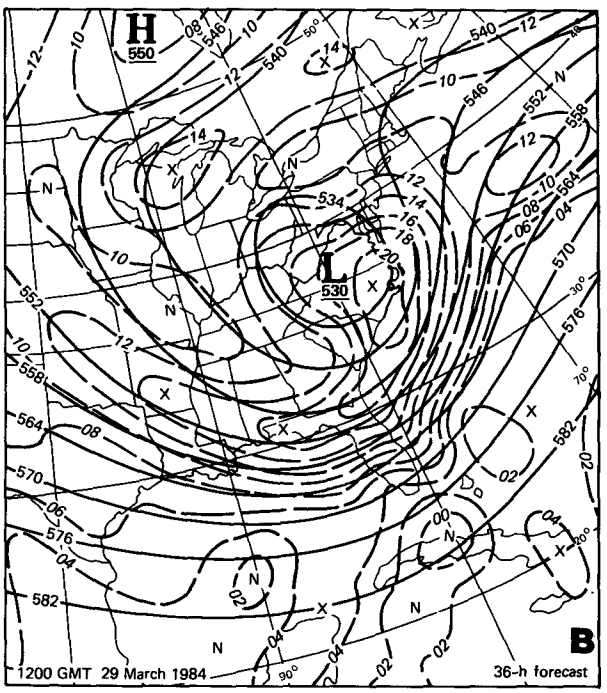

FIG. 22. As for Fig. 20, except for the 36-h forecast verifying at 1200 UTC 29 March 1984.

As further evidence of the LFM's problem in forecasting the onset of this mesocyclone, we show Fig. 23, which compares the forecast and observed precipitation. The LFM-forecast precipitation amounts are half of the facsimile precipitation forecast numbers because those LFM precipitation displays have been erroneously doubled (Phillips 1985). The thermodynamic effects of the precipitation in the LFM model, however, are unaffected by this display error. The LFM, while forecasting between 0 and 8 mm of rain throughout South Carolina, Georgia, and Alabama, misses the observed bands of precipitation in excess of 16 mm. These bands occurred along the path of the mesocyclone (Fig. 8), and our earlier discussion has suggested the importance of this convective rainfall upon this incipient cyclogenesis.

7. Concluding discussion

The March 1984 cyclogenesis represents a rare instance (Sanders and Gyakum 1980) of explosive land development. Since this cyclogenesis occurred in the midst of a relatively dense, and frequently reporting, surface data network, we have exploited the opportunity to diagnose this rapid cyclogenesis hourly.

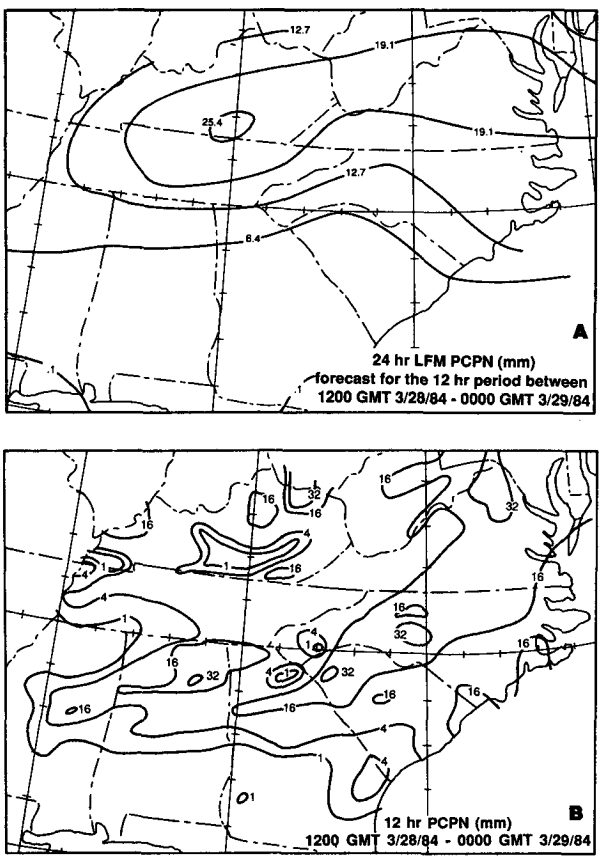

FIG. 23. (a) LFM 24-h precipitation forecast (mm) for the 12-h period ending at 0000 UTC 29 March. (b) As for (a), except for the observed precipitation.

The cyclogenesis occurred in an environment synoptically favorable for cyclogenesis, although the paucity and limited frequency of the radiosonde data precludes us from precisely relating the surface cyclogenesis location and intensity with the corresponding upper level forcing. Our hourly surface observations show the cyclone developed along an intensifying frontal zone. A substantial part of the available frontogenetic forcing was geostrophic *prior* to the formation of the surface low center. Additionally, the precursor frontogenesis was aided strongly by differential diabatic heating with intense solar heating in the clear warm air and cloudy conditions in the cooler air. The surface warming and moistening reduced the static stability in the cyclogenesis region. Surface-based lifted indices in the midst of the incipient cyclone at 1800 UTC 28 March were about −8°C.

The surface low formed at the intersection of the axes of maximum adiabatic and diabatic frontogenetic forcing and low static stability. We can reasonably argue that all three of these factors contribute to enhanced mesoscale ascent in a favorable synoptic-scale environment. Both of the frontal forcings would contribute to a thermally direct vertical circulation with rising motion in the warmer air. The reduced static stability would act to enhance this ascent. We emphasize, however, that these three processes were acting quasi-independently of one another. The precursor adiabatic frontogenesis, primarily geostrophic, is caused by the configurations of both the surface temperature field and the synoptic-scale pressure field. The diabatic frontogenesis is caused by the configurations of the surface temperature and solar heating fields. The wavelength of the heating perturbation (Fig. 14) across the developing cold front is only about 600–700 km—distinctively subsynoptic scale. The static destabilization is related mainly to the configuration of moistening and surface warming. Though these three processes may collectively aid the mesocyclogenesis, their *concurrent* appearance at the same location may be coincidental.

Deep cumulus convection, a consequence of the weak static stability and abundant moisture supply, was nearly collocated with the surface cyclone during its 4-h central pressure fall of 11 mb, and this process may have aided in the explosive cyclogenesis. This association of cumulus convection with early and unforecast synoptic-scale cyclogenesis was also found by Tracton (1973) for continental cyclogenesis, and by Gyakum (1983a) for the incipient vortex formation of the *QEII* cyclone. Our potential vorticity analysis (Fig. 18) strongly suggests a lower tropospheric generation during the cyclone's life cycle, which is consistent with the notion that diabatic processes are important to this cyclogenesis.

Although we did not investigate the relationship of orography to the surface cyclogenesis in detail, its crucial influence, in the form of vortex stretching, on explosive development is doubtful. The cyclone formed near the southern edge of the Appalachian Mountains in Alabama; its path through northern Georgia was approximately parallel to the hills oriented ~100 km to the north. The mean lower tropospheric flow was also nearly parallel to the Appalachians, which argues against orographic cyclogenesis. Additionally, the low moved rapidly with the hills to its *left,* and towards an area of orographically-induced upslope flow, vertical shrinking, and horizontal *divergence.* Thus, other processes appear to overwhelm this orographic signal.

The second pulse of rapid deepening, beginning at 0400 UTC 29 March, though briefly associated with enhanced convection near the cyclone center by 0600 UTC, may have been related more exclusively to larger scale vorticity advection. As seen in Fig. 8, the area of this specific cyclone's circulation grew considerably from 2100 UTC 28 March until 0600 UTC 29 March. Therefore, at this latter time, the cyclone would be less sensitive to both static stability and convective influences. As shown by Fig. 24, the axis of maximum 500-mb vorticity advection (deduced from 12-hourly LFM analyses and continuity of the associated cloud features on hourly satellite images) approaches the surface cyclone, as it recurves northward, by 0400 UTC 29 March.

The operational models completely missed the early mesoscale cyclogenesis studied in this paper. While the LFM should not be expected to forecast mesoscale features, the observed subsynoptic scale cyclone did grow into an important synoptic-scale low. Understanding this growth may be important to our understanding of synoptic-scale cyclogenesis. Several experiments performed with NMC's new Regional Analysis and Forecast System (Phillips 1985) have shown no success in forecasting this mesocyclone (Collins and Tracton 1985). This missed forecast may have been related to a combination of insufficient 500-mb cyclonic vorticity advection defining the synoptic-scale environment and a lack of frontally-induced rainfall. The fact that several upper-tropospheric wind observations were missing at the initial time suggests the model underestimated the wind speeds, the strength of the associated vorticity, and its advection. We did not examine the model's lower tropospheric frontal forcing or its static stability changes. However, the lack of rainfall along the cyclone's early path suggests that these processes were not well simulated.

Finally, we would like to view this work from the

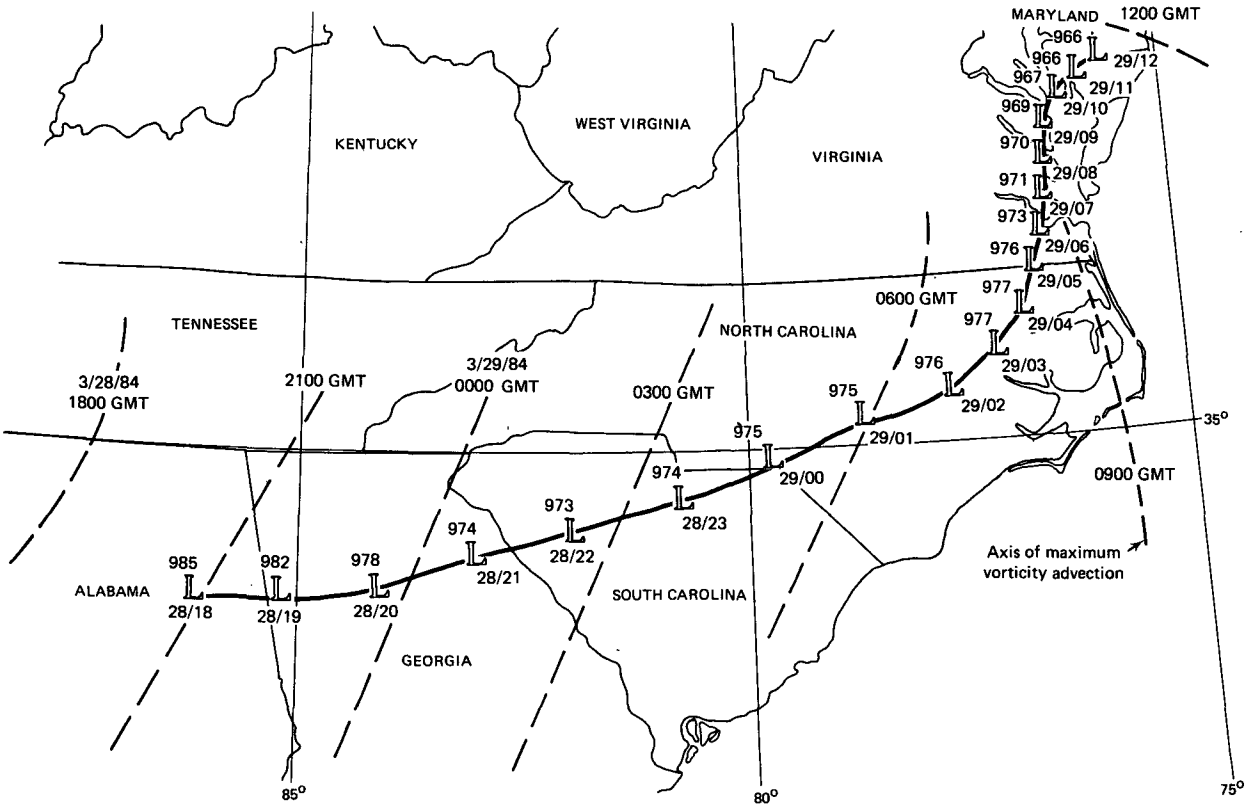

FIG. 24. Hourly positions, central pressures, dates and times of the surface low. Three-hourly positions of maximum 500-mb cyclonic vorticity advection are shown by the dashed lines.

perspective of other observational studies dealing with explosive cyclogenesis. The cyclone developed in an area of upper-level cyclonic vorticity advection, and this behavior is evidently typical of most bombs (Sanders 1986). Clearly, our finding of cumulus convection occurring close to the incipient cyclone center agrees with Tracton's (1973) conclusions. Bosart (1981) and Gyakum (1983a) have seen similar features in explosive cyclogenesis cases. Our potential vorticity analysis suggests a lower tropospheric generation due to diabatic processes; this is similar to conclusions drawn by Gyakum (1983b) and Bosart and Lin (1984).

The association of frontogenetical forcing with the cyclogenesis has also been discussed by Bosart and Lin (1984) for the President's Day cyclone, and by Reed and Albright (1986) for an explosive cyclone in the Pacific Ocean. Keshishian and Bosart (1987) have recently presented a case of an East Coast cyclone intensifying along a warm, moist and intensifying baroclinic zone.

The substantial static destabilization prior to the convection and explosive cyclogenesis has been noted by Reed and Albright (1986). Whereas the fluxes of sensible and latent heat were responsible for the destabilization in Reed and Albright's oceanic case, the strong solar heating in the moist air mass destabilized the air surrounding the March 1984 incipient cyclone.

The studies of Uccellini et al. (1984) and Uccellini (1986) have emphasized the role of jets in explosive cyclogenesis, and our synoptic analysis does show that the surface low developed in a favorable large-scale environment, characterized by its location downstream of a strong upper-level trough and jet. However, the strong signals found in three quasi-independent surface-based processes (geostrophic and diabatic frontogenesis, and static destabilization) of differing scales during the cyclogenesis also suggest their importance to cyclone development. These surface-based processes also specify a location that is conducive to explosive subsynoptic scale cyclogenesis within an area of synoptic-scale ascent. Thus, the coincident superposition of strong lower and upper tropospheric forcing appears to have forced this extreme cyclogenesis.

Modeling and additional observational studies, using enhanced surface and upper-level datasets, should be made to quantify the relative cyclogenetic role of each process discussed in this paper. However, our results suggest that explosive cyclogenesis may be a consequence of several of these processes coincidentally appearing together. The fact that the processes discussed here have also been observed in explosive oceanic cyclogenesis suggests common causes of both land and maritime bombs. The relative rarity of continental bombs may be a consequence of how infrequently favorable upper-level forcing combines with strong surface-based processes, such as frontogenesis (both adiabatic and diabatic), extreme static instability and convection, and an abundant moisture supply. Such a collection may be more common over the extratropical oceans.

Acknowledgments. This research has been supported by the National Science Foundation under Grants ATM-8305096 and ATM-8516263. John Brother and Gayle Dowell drafted the figures. Norene McGhiey and Karen Garrelts typed the manuscript. The authors would like to thank Professors Lance Bosart, Jacques Derome, Frederick Sanders, Richard Reed, Carlyle Wash, and Drs. Steve Tracton and Bill Kuo for sharing their insights about this work. We would also like to thank the personnel of the Raleigh–Durham National Weather Service forecast office and the National Climate Center at Asheville for providing supplementary cooperative surface observations. Ship and buoy observations were obtained from the National Climate Center.

APPENDIX

List of Symbols

R	gas constant for dry air
P	pressure
θ	virtual potential temperature
P_0	1000 mb
C_p	specific heat at constant pressure
κ	R/C_p
T_v	virtual temperature
$\mathbf{V}_g$	geostrophic wind vector
u_g	geostrophic wind component in the east (x) direction
V_g	geostrophic wind component in the north (y) direction
∇	horizontal gradient operator
u	eastward wind component
v	northward wind component
ϕ	latitude
a	mean Earth radius

REFERENCES

Anthes, R. A., Y.-H. Kuo and J. R. Gyakum, 1983: Numerical simulations of a case of explosive marine cyclogenesis. *Mon. Wea. Rev.*, **111**, 1174–1188.

Barnes, S. L., 1973: Mesoscale objective map analysis using weighted time-series observations. 60 pp. [NTIS Rep. No. COM-73-107 81, National Technical Information Service, Springfield, Virginia.]

Bosart, L. F., 1981: The Presidents' Day snowstorm of 18–19 February 1979: A subsynoptic-scale event. *Mon. Wea. Rev.*, **109**, 1542–1566.

——, and S. C. Lin, 1984: A diagnostic analysis of the Presidents' Day storm of February 1979. *Mon. Wea. Rev.*, **112**, 2148–2177.

Collins, W. G., and M. S. Tracton, 1985: Evaluation of NMC's Regional Analysis and Forecast System—heavy precipitation events. Preprints, *Sixth Conf. on Hydrometeorology*, Indianapolis, Amer. Meteor. Soc.

Ertel, H., 1942: Ein neuer hydrodynamischer wirbelsatz. *Meteor. Z.*, **59**, 277–281.

Gerrity, J. F., 1977: The LFM model—1976: A documentation. NOAA Tech. Memo, NWS NMC-60. [Available from the National Meteorological Center, World Weather Building, Washington, DC 20237; NTIS Rep. No. PP-279-419.]

Gidel, L. T., and M. A. Shapiro, 1979: The role of clear air turbulence in the production of potential vorticity in the vicinity of upper tropospheric jet streams-frontal systems. *J. Atmos. Sci.*, **36**, 2125–2138.

Gyakum, J. R., 1983a: On the evolution of the *QEII* storm. Part I: Synoptic aspects. *Mon. Wea. Rev.*, **111**, 1137–1155.

——, 1983b: On the evolution of the *QEII* storm. Part II: Dynamic and thermodynamic structure. *Mon. Wea. Rev.*, **111**, 1156–1173.

Hoskins, B. J., 1982: The mathematical theory of frontogenesis. *Annual Reviews in Fluid Mechanics*, Vol. 14, Annual Reviews, 131–151.

——, and M. A. Pedder, 1980: The diagnosis of midlatitude synoptic development. *Quart. J. Roy. Meteor. Soc.*, **106**, 707–719.

——, I. Draghici and H. C. Davies, 1978: A new look at the ω-equation. *Quart. J. Roy. Meteor. Soc.*, **104**, 31–38.

Keshishian, L. G., and L. F. Bosart, 1987: A case study of extended East Coast frontogenesis. *Mon. Wea. Rev.*, **115**, 100–117.

Petterssen, S., 1956: *Weather Analysis and Forecasting, Vol. I.* McGraw-Hill, 428 pp.

Phillips, N. A., 1985: Pre-implementation results from the Regional Analysis and Forecast System (RAFS). NWS Tech. Procedure Bull. No. 350, NOAA, Washington, DC, 13 pp. [Available from the National Weather Service Program Requirements and Planning Division, Silver Spring, MD 20710.]

Reed, R. J., and E. F. Danielson, 1959: Fronts in the vicinity of the tropopause. *Arch. Meteor. Geophys. Bioklim.*, **A11**, 1–17.

——, and M. D. Albright, 1986: A case study of explosive cyclogenesis in the eastern Pacific. *Mon. Wea. Rev.*, **114**, 2297–2319.

Roebber, P. J., 1984: Statistical analysis and updated climatology of explosive cyclones. *Mon. Wea. Rev.*, **112**, 1577–1589.

Sanders, F., 1986: Explosive cyclogenesis in the west-central North Atlantic Ocean, 1981–84. Part I: Composite structure and mean behavior. *Mon. Wea. Rev.*, **114**, 1781–1794.

——, and J. R. Gyakum, 1980: Synoptic-dynamic climatology of the "bomb". *Mon. Wea. Rev.*, **108**, 1589–1606.

Sawyer, J. S., 1956: The vertical circulation at meteorological fronts and its relation to frontogenesis. *Proc. Roy. Soc. London*, **A234**, 346–362.

Shapiro, M. A., A. J. Krueger and P. J. Kennedy, 1982: Nowcasting the position and intensity of jet streams using a satellite-borne total ozone mapping spectrometer. *Nowcasting*, K. A. Browning, Ed., Academic Press, 137–145.

Staley, D. O., 1960: Evaluation of potential-vorticity changes near the tropopause and related vertical motions, vertical advection of vorticity, and transfer of radioactive debris from stratosphere to troposphere. *J. Meteor.*, **17**, 591–620.

Tracton, M. S., 1973: The role of cumulus convection in the development of extratropical cyclones. *Mon. Wea. Rev.*, **101**, 573–593.

Uccellini, L. W., 1986: The possible influence of upstream upper-level baroclinic processes on the development of the QEII storm. *Mon. Wea. Rev.*, **111**, 1019–1027.

——, P. J. Kocin, R. A. Petersen, C. H. Wash and K. F. Brill, 1984: The Presidents' Day cyclone of 18–19 February 1979: Synoptic overview and analysis of the subtropical jet streak influencing the pre-cyclogenetic period. *Mon. Wea. Rev.*, **112**, 31–55.

——, D. Keyser, K. F. Brill and C. H. Wash, 1985: The Presidents' Day cyclone of 18–19 February 1979: Influence of a tropopause fold on rapid cyclogenesis. *Mon. Wea. Rev.*, **113**, 962–988.